



# The impact of process parameters and pin-to-shoulder ratio in FSW of polycarbonate: welding forces and critical quality indicators

Nectarios Vidakis<sup>1</sup> · Markos Petousis<sup>1</sup> · Constantine David<sup>2</sup> · Dimitrios Sagris<sup>2</sup> · Nikolaos Mountakis<sup>1</sup> · Amalia Moutsopoulou<sup>1</sup>

Received: 23 October 2023 / Accepted: 11 January 2024 / Published online: 25 January 2024  
© The Author(s) 2024

## Abstract

Friction stir welding (FSW) as a welding process for polymers is growing steadily, owing to its inherent advantages. The developed forces during the joining process are sensitive to the parameters used and affect the quality of the weld in terms of voids and defect formation. This study focuses on the analysis of the effects of four FSW parameters on the developed forces in joining polycarbonate (PC) 4 mm thick sheets. The porosity of the produced seams was investigated with micro-computed tomography. The dimensional deviation (top surface retreat) was also assessed with the same method. The produced seams were further inspected with microscopy. A Taguchi L9 array was formed. Analysis of variances provided prediction models for the developed forces, the porosity, the dimensional deviation, and the welding resistance rate ( $F_x/F_z$ ), which were the response metrics of the study. The model's reliability was evaluated with a confirmation run. Low travel and high rotational speeds reduce the forces in the process and lead to higher mechanical performance. Low travel speeds also reduce the porosity of the weld and affect its dimensional accuracy. The overall results offer valuable insights for optimizing the performance of FSW welds in PC sheets, which was the aim of the study (reduced porosity, dimensional deviation, etc.). The developed models ensure their successful application in real-world scenarios. Finally, the findings and the analysis were correlated with the mechanical strength of the welded PC sheets, revealing, and interpreting the mechanisms leading to higher mechanical performance of the samples.

**Keywords** Friction stir welding (FSW) · Polycarbonate (PC) · Optimization · Taguchi design · FSW forces · Porosity

## Nomenclature

ANOVA	Analysis of variances
AS	Advancing side
CCW	Counterclockwise
CNC	Computer numeric control
CW	Clockwise
DOE	Design of experiment
DSC	Differential scanning calorimetry
FSW	Friction stir welding
HAZ	Heat-affected zone
HAM	Hybrid additive manufacturing
MAPE	Mean absolute percentage error
MEP	Main effect plot
NZ	Nugget zone
PC	Polycarbonate
RS	Rotational speed
RT	Residual thickness
RTS	Retreating side
RPM	Revolutions per minute
SEM	Scanning electron microscopy

---

✉ Nectarios Vidakis  
vidakis@hmu.gr

Markos Petousis  
markospetousis@hmu.gr

Constantine David  
david@ihu.gr

Dimitrios Sagris  
dsagris@ihu.gr

Nikolaos Mountakis  
mountakis@hmu.gr

Amalia Moutsopoulou  
amalia@hmu.gr

<sup>1</sup> Department of Mechanical Engineering, School of Engineering, Hellenic Mediterranean University, 71410 Heraklion, Greece

<sup>2</sup> Department of Mechanical Engineering, International Hellenic University, Serres Campus, 62124 Serres, Greece

SV	Side view
Tg	Glass transition temperature
TGA	Thermogravimetric analysis
TMZ	Thermomechanically affected zone
TS	Travel speed
TV	Top view
WE	Weld efficiency
WT	Welding temperature
$\mu$ -CT	Micro-computed tomography

## 1 Introduction

Friction stir welding was developed as a specialized technique to join parts that are challenging to weld using traditional methods [1]. It was introduced by the British Welding Institute in 1991, mainly for aluminum parts welding [1]. The method is an autogenous welding process, featuring a non-consumable welding tool [2]. It is also considered an energy-efficient parts-joining method tool [2]. Due to these unique characteristics, the use of the process rapidly expanded and different aluminum grades [2–9] were investigated, for example, the AA5083 [10, 11], Al-5052 [12], and the AA6061 [13–20]. AA6061 has been tested also in the friction stir spot welding method, and modeling tools, such as the Taguchi design of experiments, have been applied to analyze and optimize the results [21–23]. Many results have been presented to cover a wide range of research aspects in the field [12, 24, 25]. A common subject in the research is the effect of the FSW parameters on the performance of the weld [26, 27]. Parameters, such as the weld tool geometry, rotational, and travel speed, influence the produced seams' morphology and strength [28]. These parameters should be properly adjusted, as they affect, for example, the developed forces during the welding process [29, 30], and by extent, the developed forces may result in defects in the produced seam [31]. The importance of the developed forces during the FSW process has led to the introduction of various research works reporting and correlating the FSW parameters with the performance of the weld for the aluminum material [30, 31]. Additionally, models have been proposed in the literature for the study of the developed forces, heat, and friction during the FSW of aluminum alloys [32]. Modeling tools are common for the analysis of experimental data [33], and tools such as ANOVA have also been utilized in the field [15]. The method has found application in various industries, such as in shipbuilding, household applications, aerospace, and automotive sectors [34].

An obvious expansion of the method was in polymeric materials, which are difficult to weld with conventional welding methods [35, 36], and the polymeric composites followed [37]. The initial challenge encountered in the research was assessing the feasibility of the process [38]. Then, the

same with the aluminum, which was initially studied, the effect of parameters, such as the weld tool, on the produced weld performance was assessed [39]. Research involves polymers popular in various types of applications, such as high-density polyethylene (HDPE) [40], poly(methyl methacrylate) (PMMA) [41], and acrylonitrile butadiene styrene (ABS) [42]. Polymeric composites have been investigated as well [43]. Dissimilar [44] and hybrid (metal-polymer) joints have been also attempted [45, 46]. As expected, the feasibility of welding 3D-printed polymeric parts has been investigated, with their 3D printing structure introducing additional challenges for the successful implementation of the method [47]. In the case of 3D printed parts, again the effect of the FSW parameters on the weld performance is examined [48], while hybrid joints have been achieved as well [49]. Popular polymeric materials behavior in the FSW have been reported, such as polylactic acid [50], polycarbonate (PC) [51], ABS [52], polyamide 6 [53], and poly (methyl methacrylate) (PMMA) [49, 54], and a few composites [55]. The defects in the produced seam with the FSW process on polymers are highly correlated with the developed forces during the process (same with the aluminum, presented above) [56] due to their effect on the material flow and the seam formation [57]. For example, high axial forces can lead to reduced thickness due to the outpouring from the weld nugget of the soft material [35]. Defects have consequences on the strength of the weld [58]. The developed forces can be adjusted by the welding parameters [57] (studies on polypropylene), indicating again the importance of selecting proper FSW parameters, to produce efficient seams. Forces developed are proportional to the contact shear stress, and it was found that higher tool rotational speed reduces the interfacial contact shear stress, leading to lower developed forces [51]. The heat produced is also proportional to the contact stress and it increases with the increase of the welding (travel) speed [51]. Additionally, the interfacial pressure (between the tool and the material) reduces, as the material softens [51]. The tool geometry also affects the developed forces during the process, as the literature reports [59]. Forces are usually measured experimentally, with different setups and configurations presented [60]. For the PC polymer, forces during the FSW have been investigated on 3 mm thick sheets using a dynamometer, considering the rotational and the welding speed as parameters [51]. Due to the importance of both the developed forces and the temperature when welding polymeric materials with the FSW process, simulation tools have been introduced [61].

Herein, polycarbonate (PC) polymer was investigated due to its popularity in various types of industrial applications such as optical [62], medical [63], electronics [64], and the automotive sector [65]. It has been applied in pure but also in composite form [66]. Recently, research has expanded in the 3D printing technology [67–69], and different composites

have been introduced to further improve its applicability [70–73]. Statistical tools have been applied to analyze the experimental findings in this case as well [74–77]. The 3D printing structure makes such an approach more necessary since the anisotropic behavior among other characteristics of the 3D printed parts further increases the complexity of the parameter effects analysis [78, 79].

Due to its extensive industrial use, its performance in the FSW process has merit. Therefore, it has been investigated in various aspects of the technology, apart from the developed forces during the process, mentioned above, such as in hybrid joints [80]. The effect of parameters on the performance of the weld, such as the use of lubrication [81], the orientation of the weld tool [82], the weld tool rotational speed [83], and the weld tool geometry [84] have been studied. Numerical modeling tools have also been introduced [85] to simulate the material flow [86]. Apart from the 3 mm PC sheets cited above, 10 mm sheets have also been studied, and it was found that the performance of the weld is highly sensitive to the parameters used in the FSW process [87]. The mechanical performance of the weld of 4 mm thick PC sheets in the FSW process has been reported, and the experimental findings were analyzed and optimized with statistical modeling tools [88].

Joining polymeric sheets with the FSW process is a challenging task, as shown by the literature review presented above. Additionally, the developed forces during the process have not been often investigated or correlated with other aspects of the process, such as the internal structure (porosity) of the produced seam, the dimensional accuracy (top surface retreat), and the mechanical performance of the welded parts. Herein, for the first time, the developed forces during the welding process with the FSW method of 4 mm thick PC sheets were studied. Statistical tools were applied to optimize the process. The effect of the weld tool geometry was considered, and the weld internal structure was evaluated with sophisticated  $\mu$ -CT scanning. The findings were correlated with the mechanical performance of the welds, which was assessed in a previous study [88] in an attempt to establish a connection between these aspects (forces, weld structure, and mechanical performance). Four FSW parameters were the control parameters for the investigation, i.e., weld tool travel speed (weld speed), rotational speed, shoulder, and pin diameter. The shoulder diameter is rarely investigated [89], while the shoulder-to-pin ratio is also an important parameter usually studied for the FSW of aluminum [90] and only recently assessed for the PC polymer in the literature [88]. An L9 Taguchi was compiled for the analysis. The forces, the porosity, and the dimensional characteristics (actual to nominal thickness of the produced seam) were correlated, and the analysis provided the optimum parameters. ANOVA led to the formation of prediction models for the response metrics, which were verified and

evaluated with confirmation runs [105]. Such an analysis contributes to the completeness of the work and significantly increases the merit of the provided results for wide industrial use.

## 2 Materials and methods

A flow chart outlining the algorithm of the experimental process followed in this research study is depicted in Fig. 1. The left side of the figure illustrates screenshots from the study's experimental procedures. PC sheets welded were 4 mm thick. The materials' information, along with the FSW process followed, the assessment of the thermal properties of the PC polymer using thermogravimetric analysis and differential scanning calorimetry (to validate the state of the material during the FSW process), the welding tools (i.e., their fabrication process), as well as the temperatures developed during the process (again, to validate the state of the material during the FSW process), along with the mechanical performance of the welds, are presented analytically in a previous work of this research team [88]. A parameter designated "welding resistance rate" was introduced as the ratio between the longitudinal and the vertical force, which is analogous to the friction coefficient metric without being the same.

### 2.1 FSW forces measurement

For the measurement of the forces developed during the FSW process, a 3-component dynamometer Kistler 9257BA (Winterthur, Switzerland) was fitted on the swing table of a vertical 5-axis machining center Haas VF2 (Oxnard, California, USA). This high-precision apparatus is capable of acquiring and recording the developed force components ( $F_x$ ,  $F_y$ , and  $F_z$ ), throughout the process. Raw quantitative data are provided which can be then turned into graphs along the trajectory the machine's spindle followed. Herein, a new metric was also introduced, named "welding resistance rate." The welding resistance rate was calculated as the ratio between the longitudinal and the vertical force at each point ( $F_x/F_z$ ), which is analogous to the friction coefficient.

### 2.2 Microscopy and $\mu$ -CT scanning

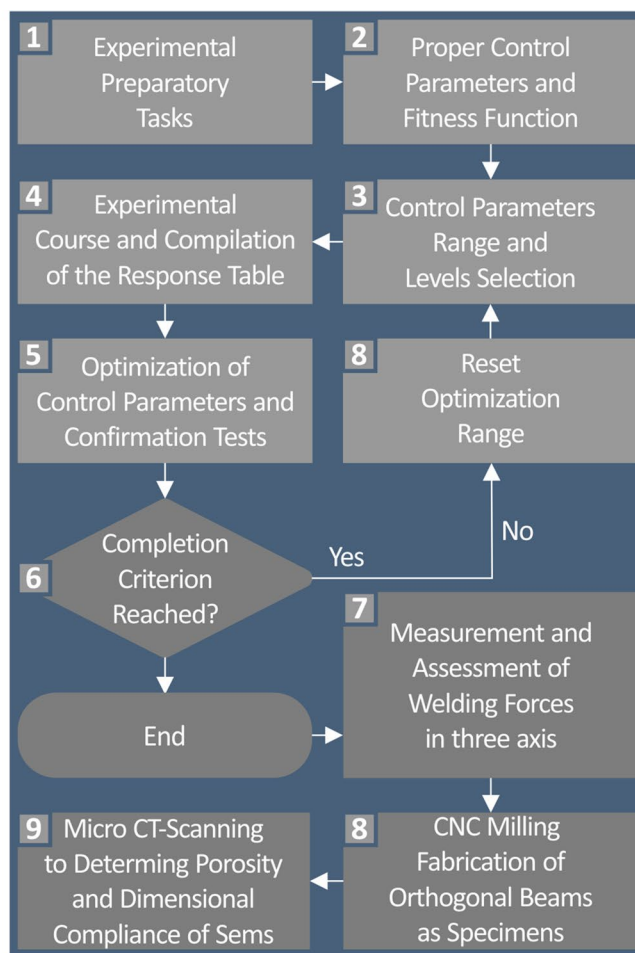
The morphological characteristics of the produced seams were inspected with a Kern OKO 1 optical microscope, equipped with the ODC 832 5MP camera (Balingen, Germany).

In this research, the weld seam internal structure, in terms of voids, porosity, and potential defects, was examined with  $\mu$ -CT scanning. The dimensional deviation at the welded region was also measured (actual to nominal thickness of the



**Fig. 1** On the right side, the steps of the experimental procedure are depicted. On the left side, images from the experimental procedure are illustrated **a** PC sheets preprocessing, **b** weld tools fabrication in

welded sample), to evaluate the retreat of the seam surface. These were achieved by employing a Tomoscope HV Compact 225 kV Micro Focus CT-scanner from Werth Messtechnik GmbH (Giessen, Germany). This CT scanner features a (1024 × 1024) pixel detector and a 225 kV micro-focused X-ray tube. Two distinct scan series were conducted: one at 60L magnification, resulting in a voxel size resolution of 60 μm, for analyzing the dimensional deviations (actual to nominal comparison of the 3D geometry), and another one at 16 μm (16L) voxel size resolution to inspect more precisely the specimen interior structure and the voids formed. The specific parameters have been set as follows: exposure time of 125 ms per step, 1600 steps per revolution of the rotary table (each 0.225°), X-ray power set at 50 W, and the acquisition of three images per step to enhance the accuracy. These parameters were selected based on the size and material density of the samples to achieve optimal image quality. The reconstructed 3D geometry of the examined samples was quantitatively and visually analyzed using the CT data



the CNC lathe, **c** fixture, **d** FSW process, **e** cutting of the samples, **f** created weld seam, **g** test samples, **h** evaluation with μ-CT scanning

set with the assistance of VG Studio MAX 2.2 software from Volume Graphics GmbH (Heidelberg, Germany).

### 2.3 Taguchi L9 design of experiment and ANOVA

In the previous study of this research team [88], a two-step Taguchi design process was implemented. First, a screening experimental process was performed, to adjust the control parameter levels. The more suitable control parameter values from this process were then employed to form a second Taguchi L9, ensuring that the values used for the study were appropriate for the process. This was verified by the acquired results and their validation with the confirmation runs. Herein, TS, RS, SD, and PD were the control parameters, and their values were selected as the ones that produced the best results in the abovementioned study, in the second Taguchi iteration, regarding the mechanical properties of the produced welds. These values were used to form an L9 Taguchi matrix for the current research, which is shown in

Table 1. The two control parameters related to the geometrical characteristics of the weld tool, i.e., SD and PD, were selected to determine the effect of the shoulder-to-pin ratio in the process. As mentioned, the shoulder-to-pin ratio has proven to be a critical parameter for the performance of the

weld of aluminum parts welded with the FSW process [90]. In polymeric parts, the shoulder-to-pin ratio only in the PC polymer has been investigated so far, to the authors’ best knowledge [88].

Next, an analysis of variance (ANOVA) was utilized, leading to the formulation of equations for the six (6) response measures, i.e.,  $F_x$ ,  $F_y$ ,  $F_z$ , porosity, dimensional deviation (actual to nominal), and welding resistance rate. Subsequently, the produced equations’ anticipated precision was computed, and their dependability was assessed through a confirmation run.

**Table 1** Taguchi L9 design: control parameters and levels

Run	TS (mm/min)	RS (rpm)	SD (mm)	PD (mm)
1	2	600	8	2
2	2	800	9	3
3	2	1000	10	4
4	4	600	9	4
5	4	800	10	2
6	4	1000	8	3
7	6	600	10	3
8	6	800	8	4
9	6	1000	9	2

### 3 Results

#### 3.1 $\mu$ -CT scan results: dimensional deviation

In Fig. 2, screenshots from the acquired 3D geometry with the  $\mu$ -CT scanner of one welded specimen per run are depicted. In each image, the weld region is magnified and

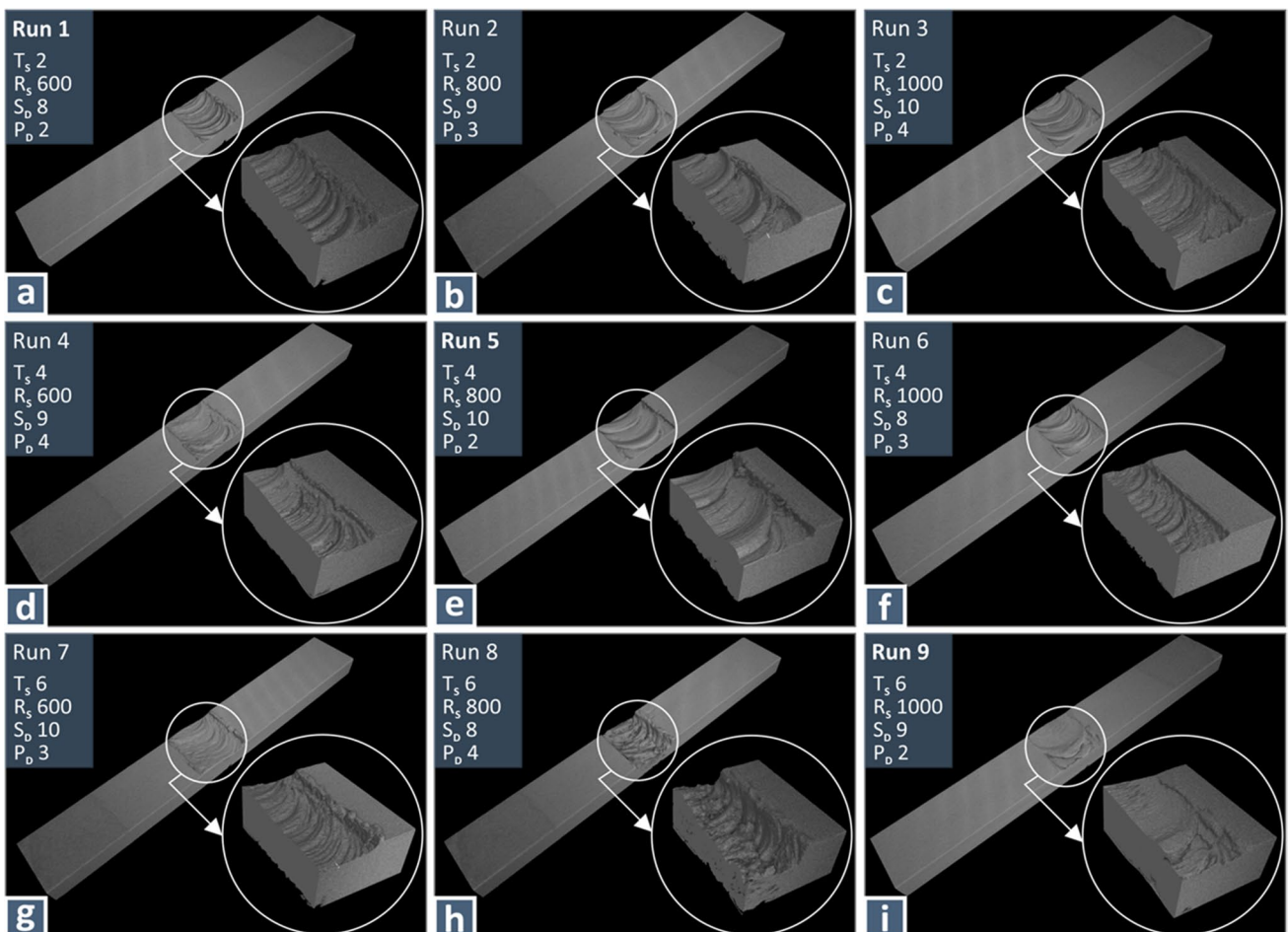


**Fig. 2** One sample from each run, as shown by the  $\mu$ -CT scanning. In each sample, the weld region is presented magnified in the corresponding inset image

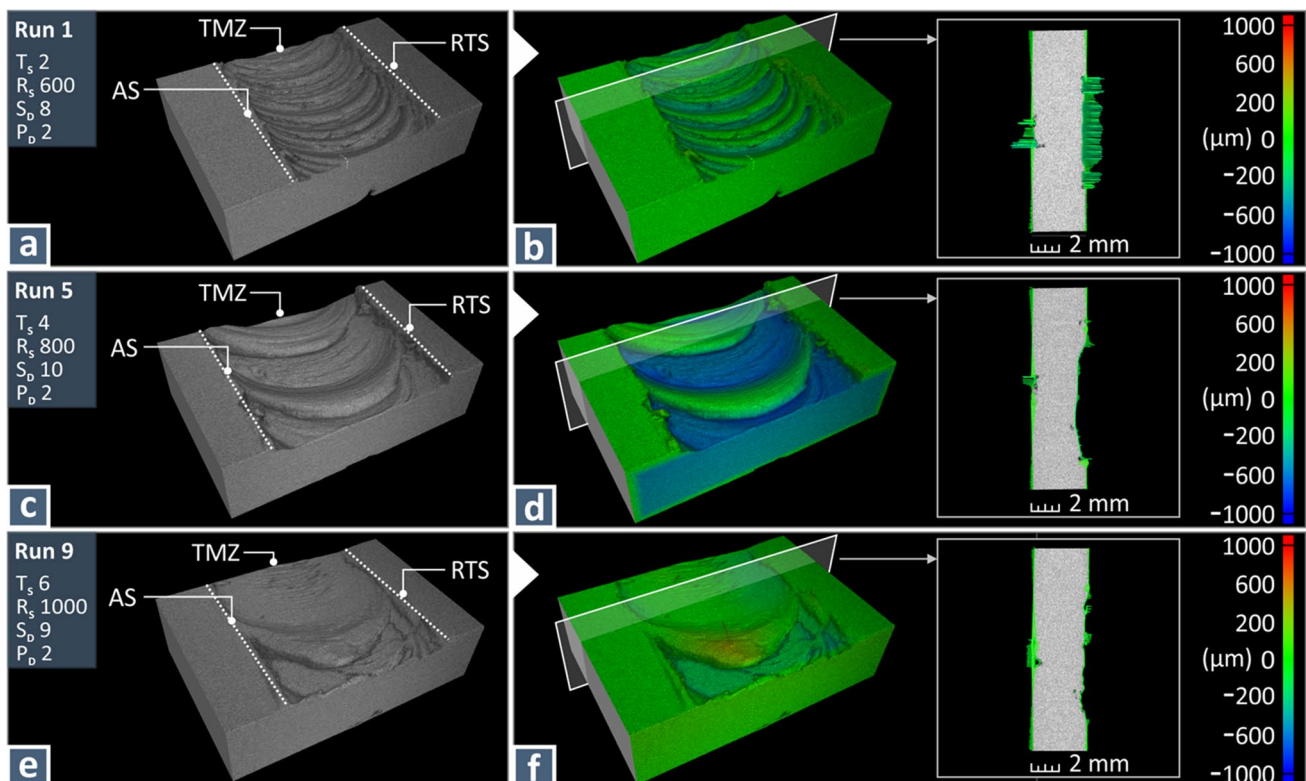
presented as an inset image to highlight the differences in the weld pattern due to the different FSW settings in each run. From the initial visual inspection, some welds appear to have a smooth pattern (Run 3), others to be rougher (Run 8), others to have a consistent circular pattern (Run 1), etc. Following the study, the runs in the diagonal of the L9 array were further assessed (Runs 1, 5, and 9), as these three runs involve control parameter values from the entire range assessed herein.

Figure 3 presents  $\mu$ -CT images focused on the weld region for the three aforementioned runs on the diagonal of the L9 (1, 5, and 9). The dimensional deviation is presented with a color-coded chart, while the circular FSW pattern and the differences between the three runs are more clearly depicted. All control parameters have higher values in Run 9, median values in Run 5, and lower values in Run 1. The circular pattern is more condensed in Run 1 and is becoming sparser in Run 5 and even more in Run 9. The dimensional deviation seems to be smaller in Run 9 and higher in Run 5. To have more concrete results on the dimensional deviation, the data acquired from the  $\mu$ -CT scanning process are quantified in Fig. 4, in which their distribution is also presented. As shown, Run 9 has the lowest dimensional deviation in absolute value but has the highest positive deviation (points higher than the nominal thickness of the sample) and the

second higher negative deviation (surface retreat). Run 1 has the second lowest dimensional deviation in absolute value and the second higher positive deviation, featuring also the lowest negative deviation. Run 5 has the highest absolute deviation and the highest negative dimensional deviation, featuring the lowest positive dimensional deviation as well. Such differences show the importance of the FSW parameters in the formed weld seam, especially since the negative deviation means a smaller cross-section on the sample and thus lower loading bearing for the sample.

### 3.2 $\mu$ -CT scan results: porosity

Figure 5 presents quantitative data related to the porosity of the weld region, as they were determined with the  $\mu$ -CT scanning process. More specifically, the number, the size, and the sphericity of the voids, along with their distribution are depicted for the three indicative runs (1, 5, and 9). The upper part shows the size distribution of the voids for the three runs. Runs 1 and 5 have a rather similar structure in terms of void number and distribution. Run 9 voids have a larger range of sizes, and the voids are extended to larger sizes than the other two runs. The bottom part of the figure shows the total number of voids per run. Run 5 has fewer voids than the other runs, while Run 9 has more voids than



**Fig. 3** Dimensional deviation of the thickness of the produced welds compared to the nominal cross-section of the sample. The characteristic regions of the weld are indicated (AS, TMZ, RTS) along with the FSW settings for each run depicted, **a, b** Run 1, **c, d** Run 5, and **e, f** Run 9

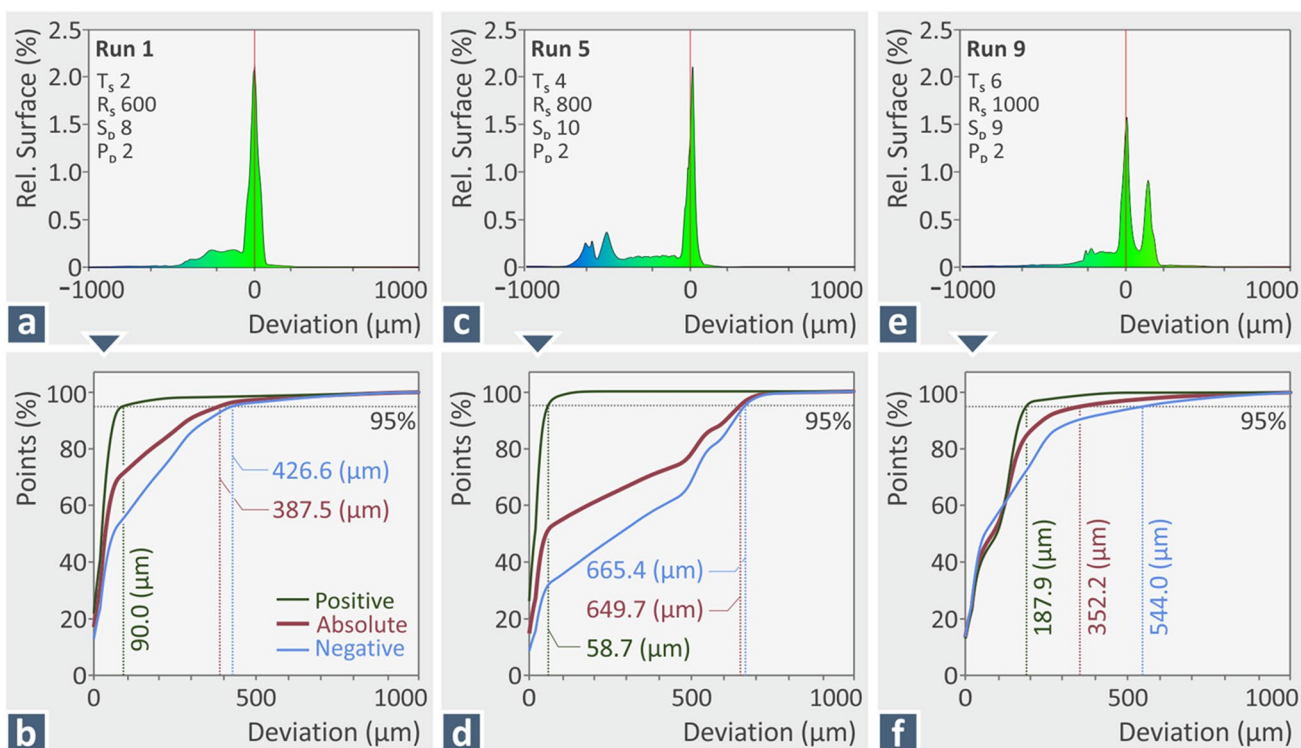


**Fig. 4** Quantification of the dimensional deviation of the samples depicting the deviation distribution and the percentage of points with positive, absolute, and negative deviation, respectively for **a, b** Run 1, **c, d** Run 5, and **e, f** Run 9

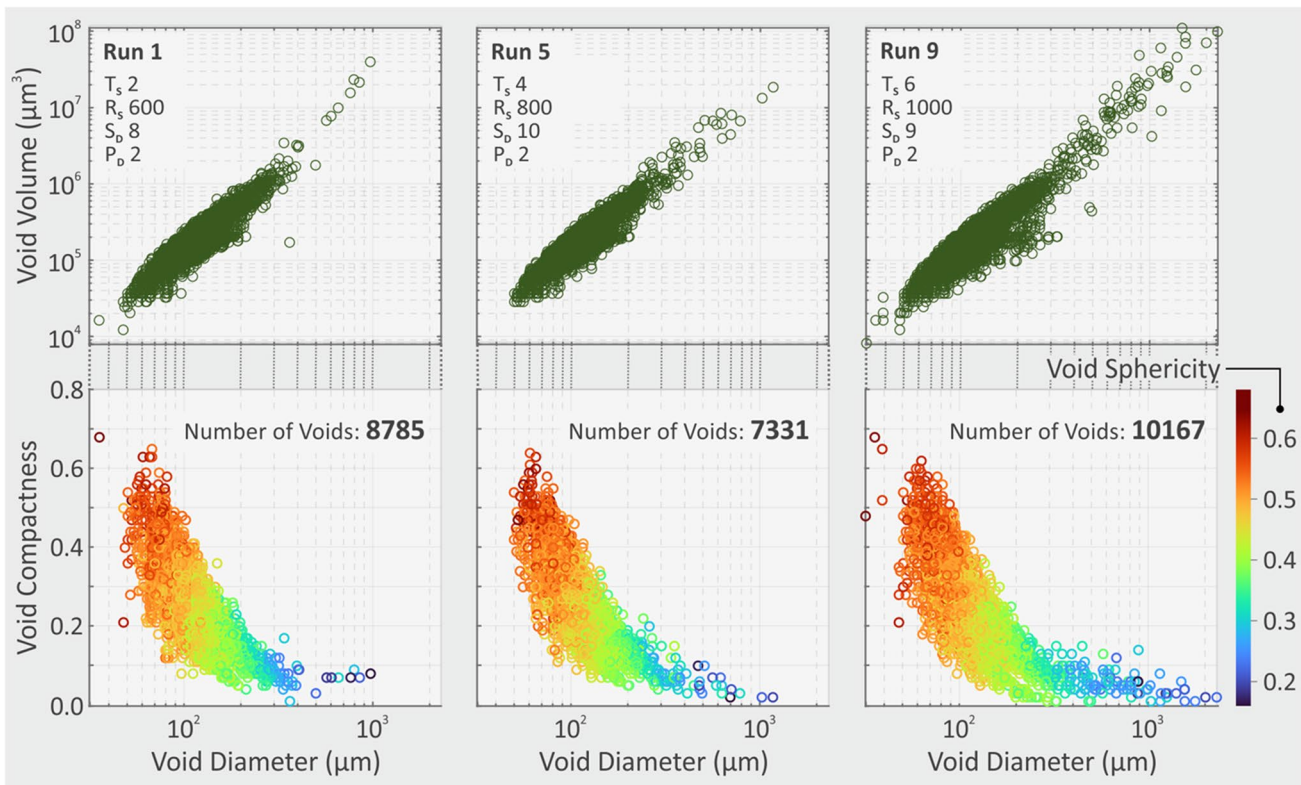


**Fig. 5** Distribution of the voids' volume (upper part of the image), size, and shape (lower part of the figure) for Runs 1, 5, and 9

the other two runs. Again, it is shown that their size (Run 9) is extended to larger diameters than the other two runs. Also, Run 5, although having fewer voids than Run 1, from their distribution, it is shown that it has more than Run 1 voids with larger size. A color scale depicts the deviation of the voids' shape from the spherical shape. In all three runs, smaller in diameter voids have larger deviations from the spherical shape, and as the size of the voids increases, they tend to better approximate the spherical shape. Finally, smaller in size voids are more compact, while, as their size increases, the larger in size voids are more scattered. Figure 6 shows a cross-section at the weld region for (a) Run 1, (b) Run 5, and (c) Run 9, visualizing the voids formed, their size, and their distribution. The void analysis results were acquired by means of the  $\mu$ -CT scan software tool.

### 3.3 FSW forces

Figures 7 and 8 show the developed force distribution in the three directions ( $F_x$ ,  $F_y$ , and  $F_z$ ) along the seam for Run 7 and Run 5, respectively. For Run 7 (Fig. 7), forces exhibit a disturbance at the beginning of the seam, where the welding tool enters the sample, and then they have a rather smooth profile, without large deviations. The highest force is developed in the vertical direction ( $F_z$ ). The force in the transversal direction ( $F_y$ ) is about an order of magnitude lower, while the force in the longitudinal direction ( $F_x$ ) is about two times the force in the transversal direction ( $F_y$ ). The highest variation in the forces is about the same ( $\sim 20$

N) in all directions. The disturbances in the forces appearing in the graphs, as they were recorded by the dynamometer, are in good agreement with the formation of the circular patterns in the FSW seam. This is the case for Run 5 as well (Fig. 8). Still, in this case, the disturbances in the forces are much higher, especially in the vertical direction, in which the developed force varies from approximately 40 to 160.16 N (higher than the  $F_z$  of Run 7, with much higher deviation). The force in the transversal direction ( $F_y$ ) is much lower but higher than the force in the longitudinal direction ( $F_x$ ) in this case and with higher deviation as well. These forces profile results in a rougher pattern for the FSW seam formed. By observing the graphs, forces in all three directions are high at the beginning of each circular pattern, they decrease along it and increase again with a peak at the beginning of the next one, and so on. This shows a high correlation between the developed forces and the surface pattern of the weld seam, which also affects the dimensional accuracy of the seam (cross-section dimensional deviation), as mentioned above. Figure 9 presents two examples of welds achieved with good (Runs 4 and 7) and inferior quality (Runs 3 and 8) welds when visually inspected. The welds with inferior quality showed inferior mechanical performance as well [88].

### 3.4 Taguchi L9 design of experiment experimental results

To quantitatively analyze the experimental results and determine the effect of the control parameter levels on

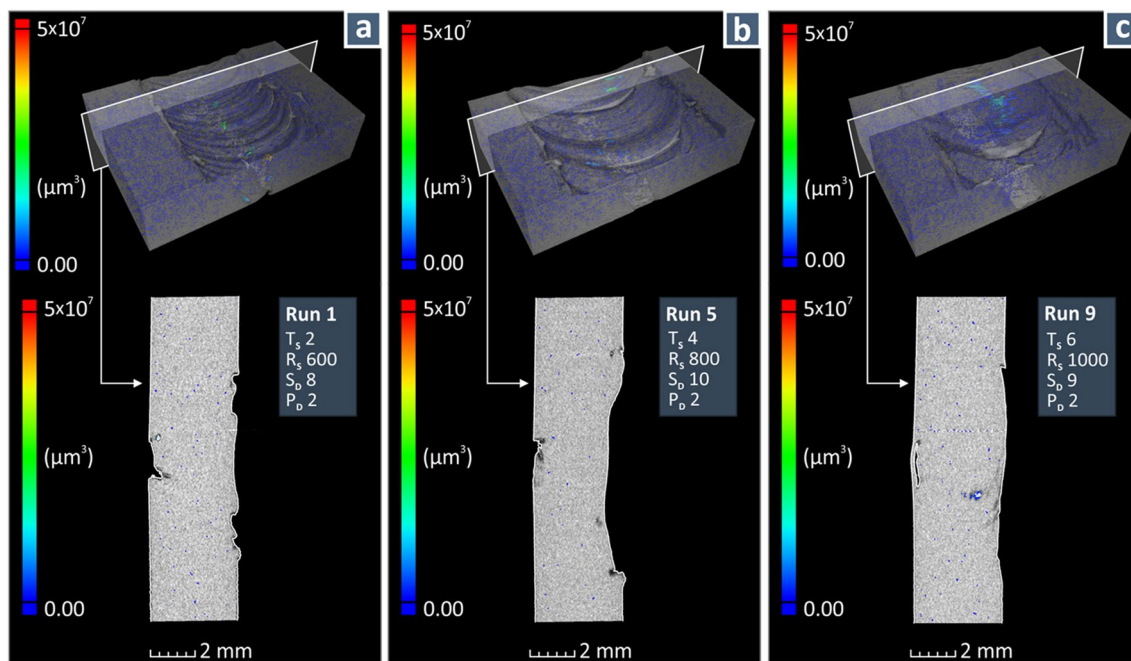


**Fig. 6** Distribution of the voids in a random cross-section of the weld presented in color code for **a** Run 1, **b** Run 5, and **c** Run 9



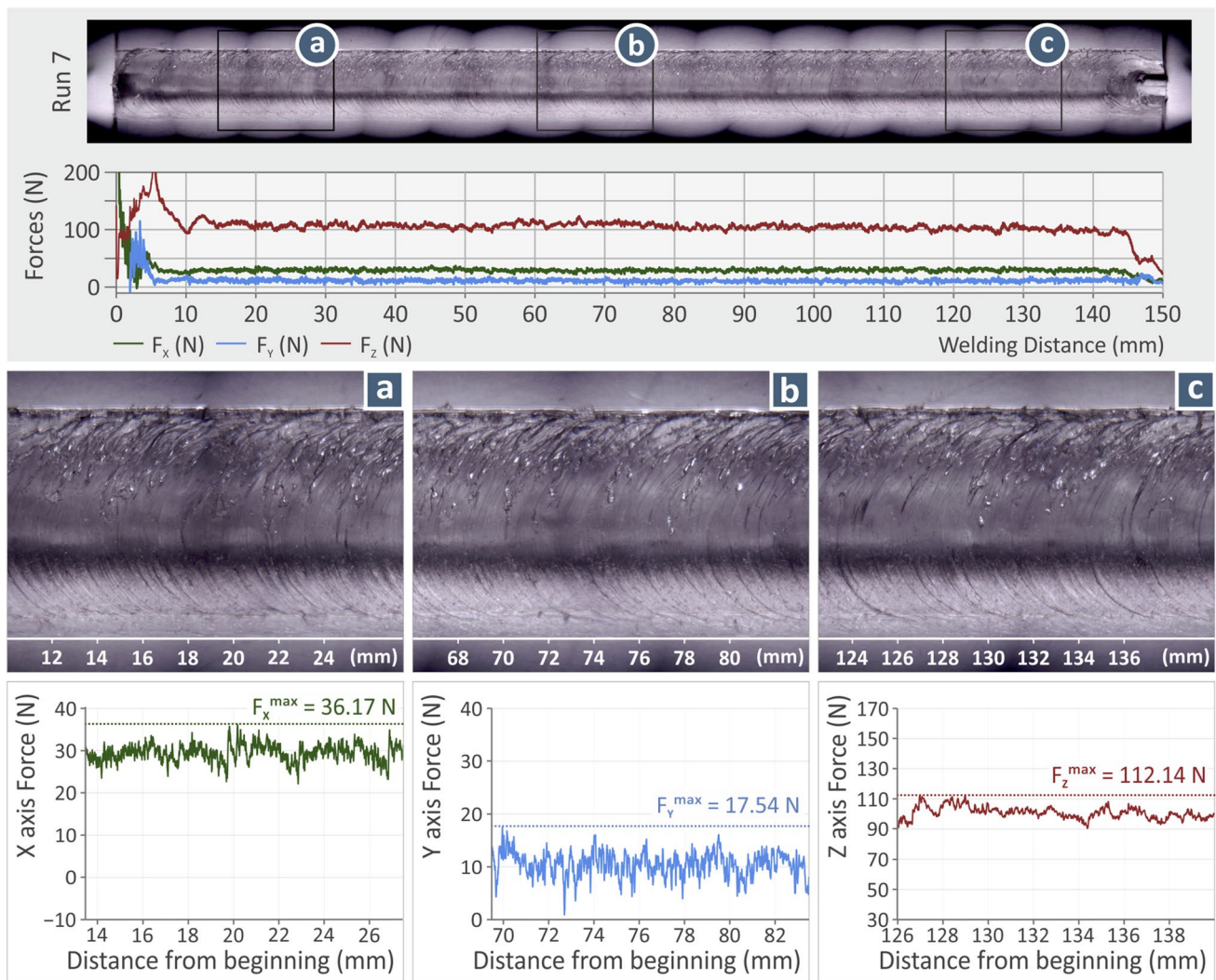


**Fig. 7** Force distribution along the weld seam for Run 7 and magnified graphs at random segments **a** at the beginning of the seam ( $F_x$ ), **b** in the middle ( $F_y$ ), and **c** at the end of the seam ( $F_z$ )

the response metrics, the average value and deviation of the response metrics are presented in Table 2. Forces  $F_x$  and  $F_y$  have values that do not significantly differ, although the lowest and the highest values were not found on the same run for these two metrics, and the  $F_x$  forces have higher deviation.  $F_z$  forces are overall significantly higher. No clear pattern and correlation between the developed forces and the porosity, the dimensional deviation, and the welding resistance rate can be found at this stage of the analysis, so further analysis is required to derive such results.

To assess the effect of each control parameter (and level) on the response metrics, MEP was formed and is presented in the following Figs. 10, 11, and 12. Figure 10 depicts MEP for the three-force metrics. In all three forces, the  $R_s$  is ranked as the no. 1 parameter in importance, with its

increase leading to a reduction in the forces' value. Apart from that, no other common observation can be derived for the forces.  $P_D$  is ranked as the no. 2 parameter in importance for the  $F_x$  and the  $F_y$  metric (no. 3 for the  $F_z$  metric), having the opposite effect between them. Its rise increases  $F_x$  and decreases  $F_y$ , while it has an overall mild effect on  $F_z$ .  $S_D$  has overall a mild effect on  $F_x$  (ranked as no. 4 in importance) and  $F_z$  (ranked as no. 2 in importance), while its median value decreases  $F_y$  (ranked as no. 4 in importance).  $T_s$  is ranked as no. 3 in importance for the  $F_x$  and the  $F_y$  metrics, while it is ranked as no. 4 in importance for the  $F_z$  metric. Its increase increases  $F_x$  and decreases  $F_y$ , while it has an overall mild effect on  $F_z$ .

Regarding the actual to nominal metric and the porosity (Fig. 11),  $T_s$  is ranked as the no. 1 important control parameter. Its rise increases the porosity and decreases the

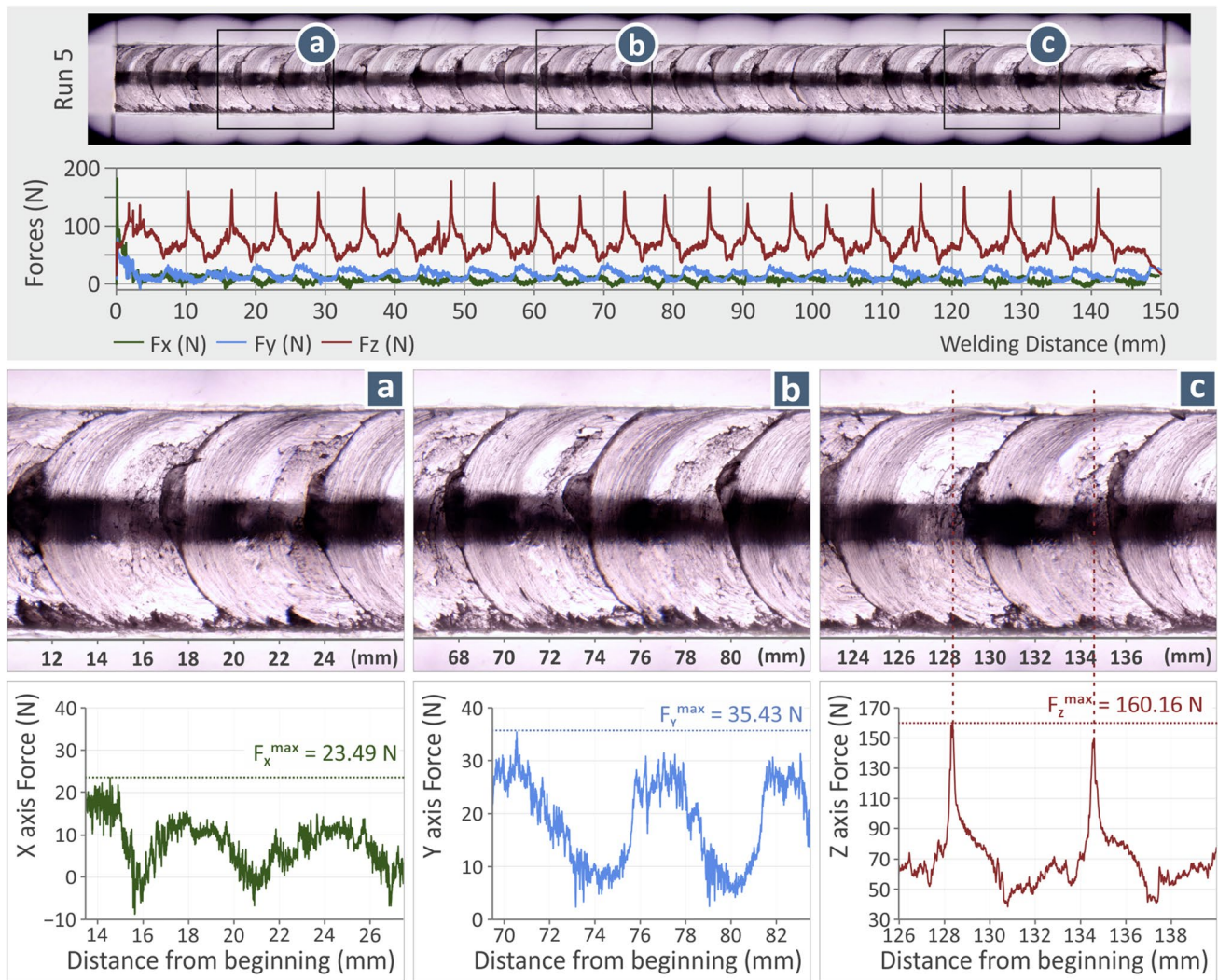


**Fig. 8** Force distribution along the weld seam for Run 5 and magnified graphs at random segments **a** at the beginning of the seam ( $F_x$ ), **b** in the middle ( $F_y$ ), **c** at the end of the seam ( $F_z$ )

dimensional deviation. For these two response metrics, the “smaller the better” criterion is the required one.  $P_D$  is ranked as no. 2 in importance control parameter, with its increase reducing the porosity and increasing the dimensional accuracy.  $S_D$  is ranked as no. 3 in importance control parameter, with its increase again reducing the porosity and increasing the dimensional accuracy. Finally,  $R_s$  is the least important among the four control parameters (ranked no. 4), having a mild effect on the porosity and its increase reducing the dimensional deviation. Figure 12 shows the MEP for the developed temperature during the FSW process (data retrieved from [88]) and the calculated welding resistance rate metric. In three of the four control parameters, the two metrics have a similar response, with the increase of  $T_s$  and  $P_D$  increasing the two metrics, and the  $R_s$  leading to lower metric values. Only in the  $S_D$  control parameter

does the response of the two metrics differ, with higher values resulting in reduced welding resistance rate and lower temperature values recorded with the median  $S_D$  control parameter value. To further assess the relationship between the control parameters in each response metric, interaction plots were formed and are provided in the supplementary material of the study.

### 3.5 ANOVA

The linear regression model (LRM) for each response is calculated as follows:

$$Y_k = a_k + \sum_{i=1}^n b_{i,k}x_i + e_k \quad (1)$$

**Fig. 9** Good quality welds (Runs 4 and 7) and welds with visually inferior quality (Runs 8 and 3)

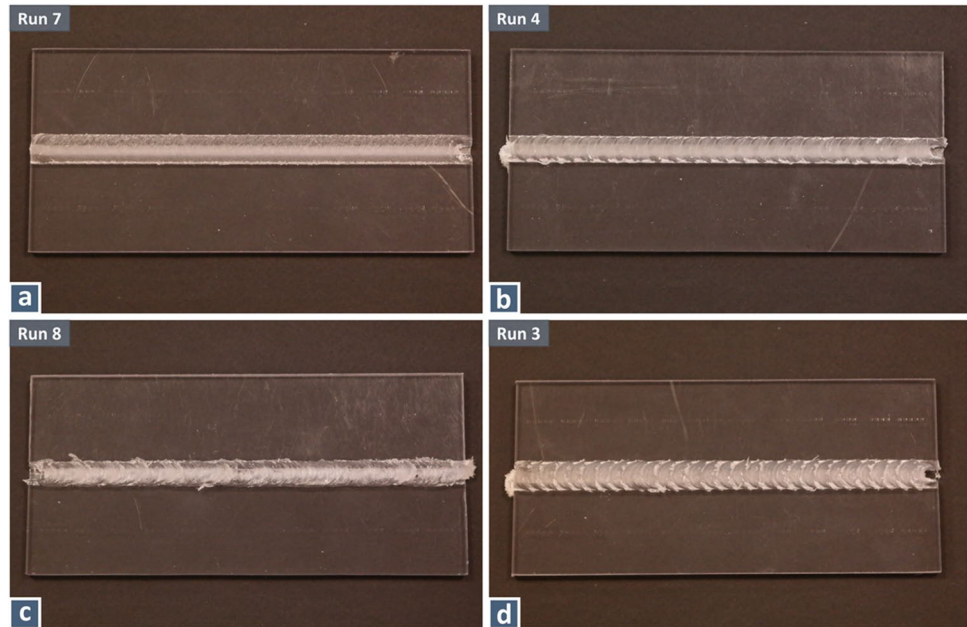


**Table 2** Mean average values and standard deviations of measured responses for the force in the X axis, force in Y axis, force in Z axis, porosity, actual to nominal dimensional deviation, and  $\mu$  (friction)

Run	Force X (N)	Force Y (N)	Force Z (N)	Porosity (%)	A2N@95% ( $\mu\text{m}$ )	$\mu$
1	15.52 ± 0.73	22.02 ± 0.48	101.12 ± 5.52	0.37 ± 0.01	381.02 ± 4.61	0.154 ± 0.007
2	11.99 ± 0.98	12.03 ± 0.74	55.39 ± 3.30	0.31 ± 0.02	388.16 ± 9.00	0.216 ± 0.013
3	12.73 ± 0.48	8.43 ± 0.62	56.17 ± 4.06	0.32 ± 0.01	414.25 ± 8.71	0.228 ± 0.022
4	24.53 ± 0.57	9.15 ± 0.34	102.49 ± 3.40	0.34 ± 0.02	395.04 ± 4.63	0.240 ± 0.011
5	8.01 ± 0.66	15.37 ± 0.68	72.28 ± 5.85	0.37 ± 0.02	395.72 ± 5.04	0.112 ± 0.016
6	8.01 ± 0.64	6.32 ± 0.41	48.49 ± 4.05	0.35 ± 0.01	368.35 ± 5.51	0.167 ± 0.025
7	28.53 ± 0.58	11.72 ± 0.64	104.82 ± 4.74	0.41 ± 0.01	378.24 ± 2.55	0.272 ± 0.011
8	21.87 ± 0.54	11.01 ± 0.37	56.43 ± 3.76	0.43 ± 0.01	375.63 ± 5.12	0.389 ± 0.019
9	11.67 ± 0.77	7.55 ± 0.28	59.24 ± 3.29	0.44 ± 0.01	329.97 ± 4.33	0.198 ± 0.023

where  $k$  represents the quality output (e.g., Force in X axis, Force in Y axis, Force in Z axis, porosity, actual to nominal dimensional deviation,  $\mu$  (friction coefficient)),  $a$  is the constant value,  $b$  is the coefficients of the linear terms,  $e$  is the error, and  $x_i$  the six ( $n = 4$ ) control parameters, i.e., the welding tool shoulder diameter and pin diameter, the welding travel and rotation speed.

The ANOVA tables for the response metrics of the study are provided in the supplementary data. For the  $F_x$  metric,  $F$ -values are more than acceptable, except for the SD control parameter and so are the  $P$ -values which approximate zero (except for the SD control parameter again).  $R$  values reported higher than 87.2%, showing the sufficiency of the model to predict the specific metric. The same observations were found for the  $F$  and the  $P$  values for the  $F_y$  metric, while  $R$  values higher than 70.70% were found, which is also an acceptable result. For the  $F_z$  metric,  $F$  and  $P$  values are not acceptable

for the  $T_s$  and the  $P_D$  control parameters. On the other hand,  $R$  values reported higher than 77.97%, showing the sufficiency of the model to predict the specific metric. Regarding the porosity,  $F$  and  $P$  values are not sufficient for the  $R_s$  control parameter.  $R$  values higher than 71.21% are reported. For the dimensional deviation,  $F$  and  $P$  values are sufficient for prediction.  $R$  values higher than 73.49% are reported. Finally, for the welding resistance rate,  $F$  and  $P$  values are not acceptable for the  $R_s$  control parameter.  $R$  values higher than 68.30% are reported, which is the lowest among the response metrics but still sufficient for prediction. Based on these tables, the prediction models for the response metrics were formed, as a function of the control parameters [91] and are presented in the following Equations (2)–(7):

$$F_x = 14.94 + 1.819 \cdot TS - 0.03014 \cdot RS + 0.645 \cdot SD + 3.987 \cdot PD \tag{2}$$

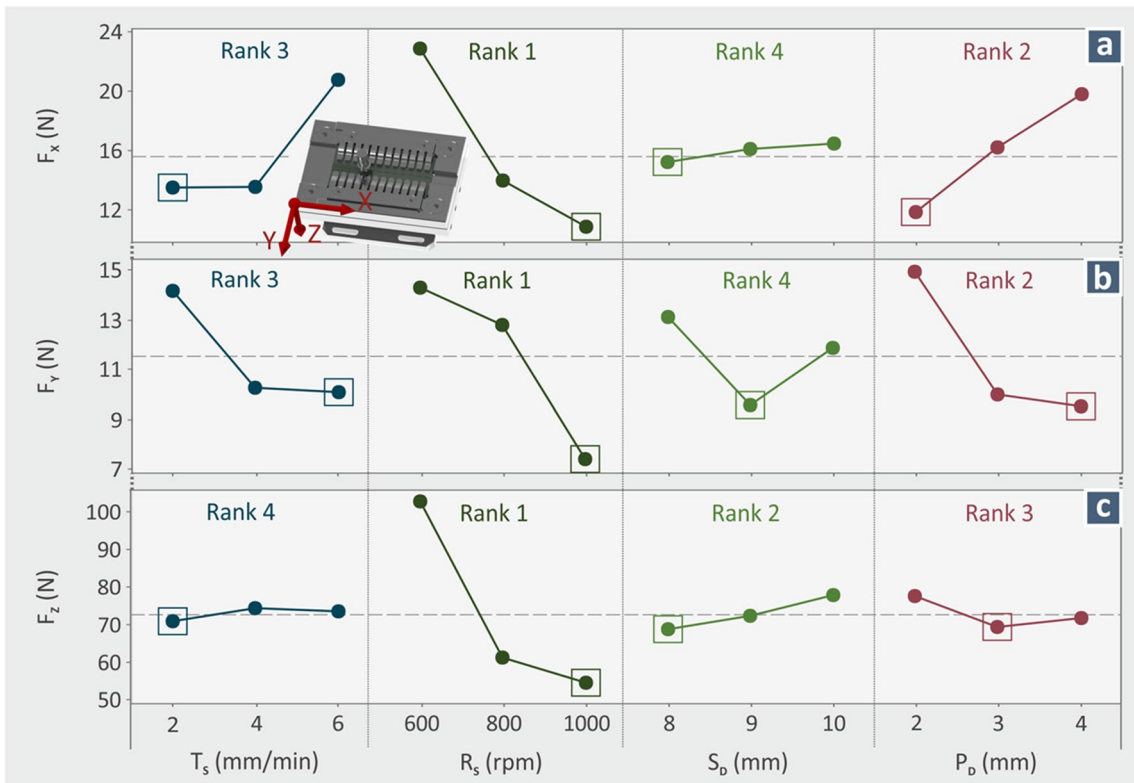


Fig. 10 MEP for a  $F_x$ , b  $F_y$ , and c  $F_z$

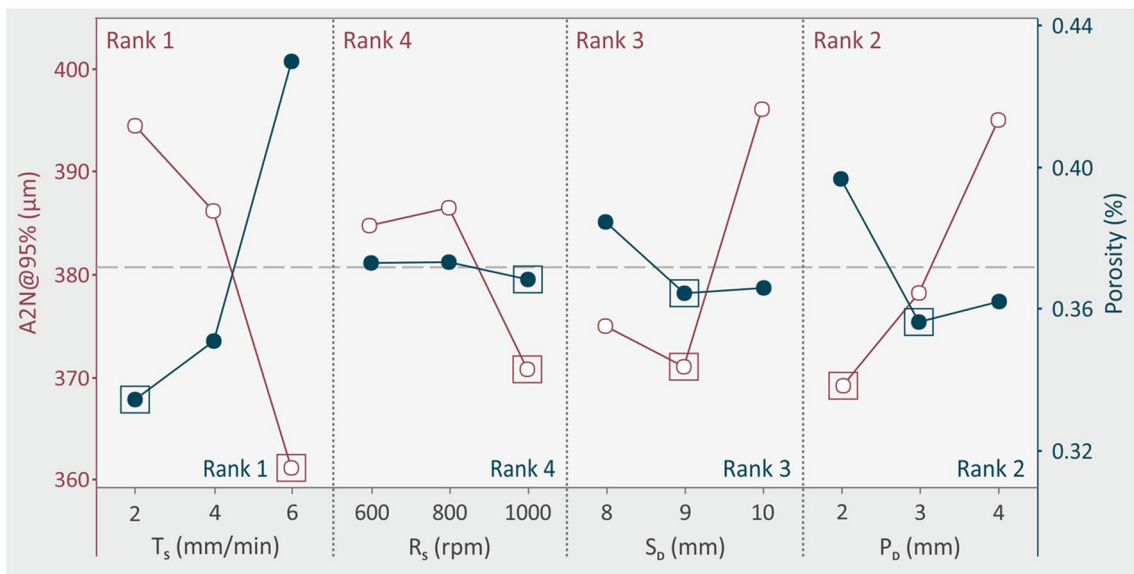


Fig. 11 MEP for actual to nominal dimensional deviation (red lines) and porosity (teal lines)

$$F_y = 43.23 - 1.016 \cdot TS - 0.01716 \cdot RS - 0.639 \cdot SD - 2.726 \cdot PD \quad (3)$$

$$Porosity = 0.4224 + 0.02367 \cdot TS - 0.000012 \cdot RS - 0.00933 \cdot SD - 0.01733 \cdot PD \quad (5)$$

$$F_z = 134.6 + 0.650 \cdot TS - 0.12045 \cdot RS + 4.54 \cdot SD - 2.93 \cdot PD \quad (4)$$

$$A_{2N@95\%} = 307.8 - 8.30 \cdot TS - 0.0348 \cdot RS + 10.53 \cdot SD + 13.04 \cdot PD \quad (6)$$

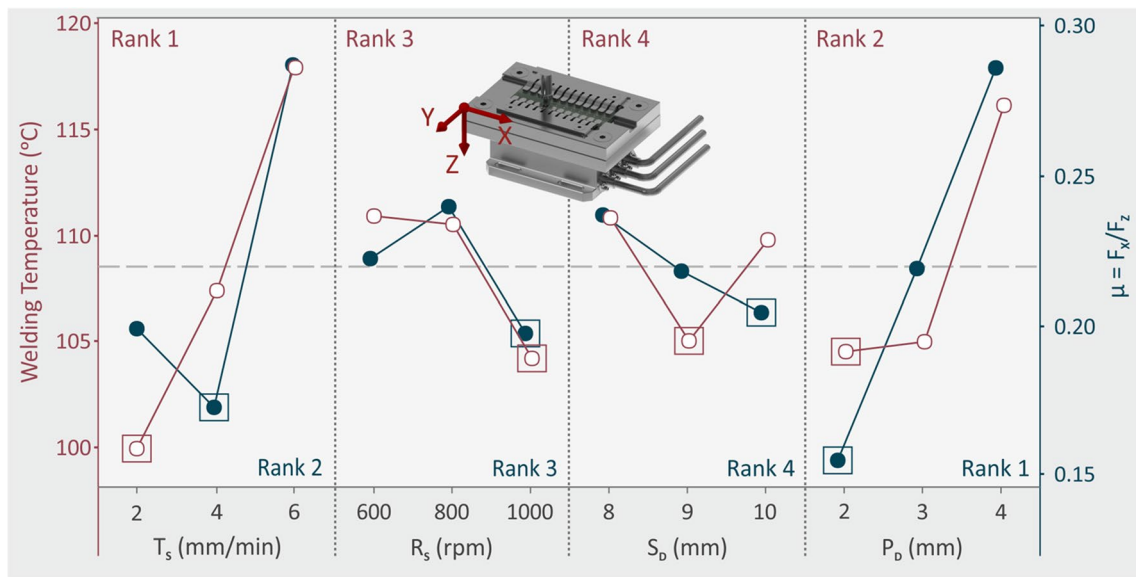


Fig. 12 MEP for the welding temperature (red lines) and welding resistance rate (friction indicator, teal lines)

$$\mu = 0.1303 + 0.02176 \cdot TS - 0.000061 \cdot RS - 0.01615 \cdot SD + 0.06541 \cdot PD \quad (7)$$

The Pareto charts were created to illustrate the key control factors with significant statistical influence on each response measure. Alongside the Pareto charts, graphs were generated comparing actual values to predicted values, demonstrating the convergence between them. In this context, two metrics were computed: the average absolute proportion error (MAPE) [92] and the Durbin-Watson statistic (indicating positive autocorrelation if it is less than 2, neutral autocorrelation if it is between 2 and 3, or negative autocorrelation if becomes greater than 3 [93]). The predictive models for all response metrics were examined, and they proved to be highly reliable as the results surpassed acceptable standards. For the dimensional deviation metric (Fig. 13a), all the control parameters were found to be statistically important. The MAPE factor was found to be 2.20% which is an exceptional result, while the Durbin-Watson statistic was 2.36 showing a neutral autocorrelation of the results. For the porosity metric (Fig. 13b), all the control parameters, except  $R_s$ , were found to be statistically important. The MAPE factor was found to be 5.38% which is a very good result, while the Durbin-Watson statistic was 1.86 showing a positive autocorrelation of the results. For the welding resistance rate metric (Fig. 14), all the control parameters, except  $R_s$ , were found to be statistically important. The MAPE factor was found to be 16.62% which is an acceptable result, while the Durbin-Watson statistic was 1.41 showing a positive autocorrelation of the results. Additional Pareto charts are included in the supplementary material of the study. In Fig. 15, a

three-dimensional surface graph portrays the relationships between the response metrics and the two most influential control parameters for each metric.

### 3.6 Confirmation run

One more test run (Run 10) was conducted to assess the precision of the predictive models. The control parameter settings for the validation run can be found in Table 3. Table 4 shows the response metrics' average values and deviations as they were derived from the confirmation run. Analytically, the experimental results from the confirmation run for each replica are presented in the supplementary data of the research. Table 5 is a validation table, presenting the actual and the predicted values of the response metrics and the difference (error) between them. As shown, in all response metrics, the accuracy is more than acceptable. Only on the welding resistance rate, the deviation between the actual and the predicted value is higher (24.19 %), still within acceptable limits. Such a higher deviation was anticipated for the specific metric, considering the ANOVA results, in which the outcome showed that higher deviations should be expected.

## 4 Discussion

Four FSW parameters, two related to the welding conditions and two to the weld tool geometry, were studied, with their levels already being optimized in a previous study with a screening Taguchi process [88]. The quality of the weld differs according to the weld conditions. The

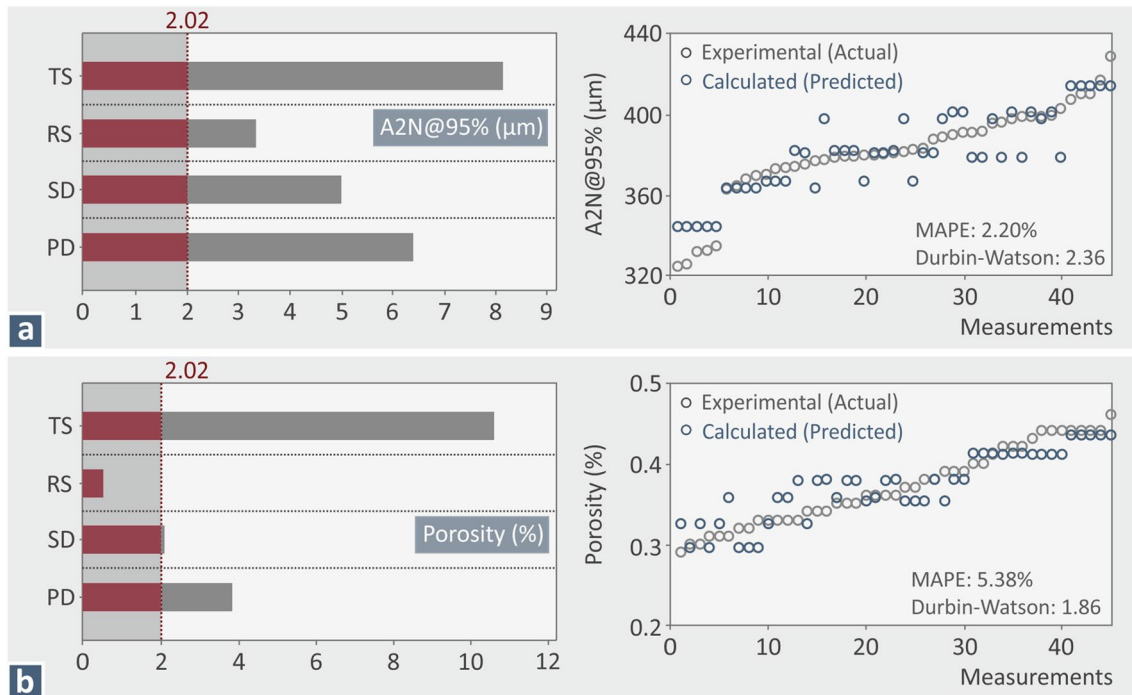


**Fig. 13** The Pareto chart and predicted vs. actual graph for **a** actual to nominal dimensional deviation and **b** porosity

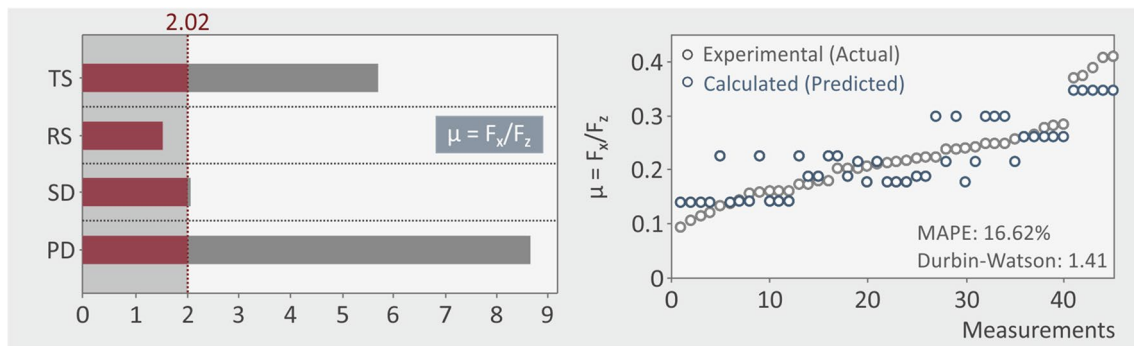


**Fig. 14** The Pareto chart and predicted vs. actual graph for the welding resistance rate (friction indicator)

statistical analysis followed suggested the optimum conditions among the ones studied. The optimization of the mechanical performance was the subject of a previous study [88]. The study herein focused on the developed forces during the FSW process, and the results were correlated with the respective mechanical test results of each case to find a possible correlation between the forces and the mechanical performance. In specific runs, the weld showed inferior quality, while in others, the weld quality was good. No significant differences were found between samples welded with the same conditions. This indicates that the conditions during the weld process are the ones affecting the quality of the weld. The inferior quality welds have an effect on the mechanical performance as was reported in this previous

study, in which a screening process was followed to derive the control parameter levels that achieved better results. All the issues faced in the screening process are presented in this previous work. Therefore, no major issues were faced herein in the FSW process of the PC sheets. The control of the welding process is achieved by maintaining constant weld parameters in each case. This is achieved by the equipment used, through the computer numeric control technology. The control parameters achieving better results were the subject of this study regarding the developed forces, the porosity, and the dimensional accuracy, and the previous study regarding the mechanical performance of the samples.

The developed forces during the FSW processing of 4 mm thick PC sheets were measured, and a sophisticated

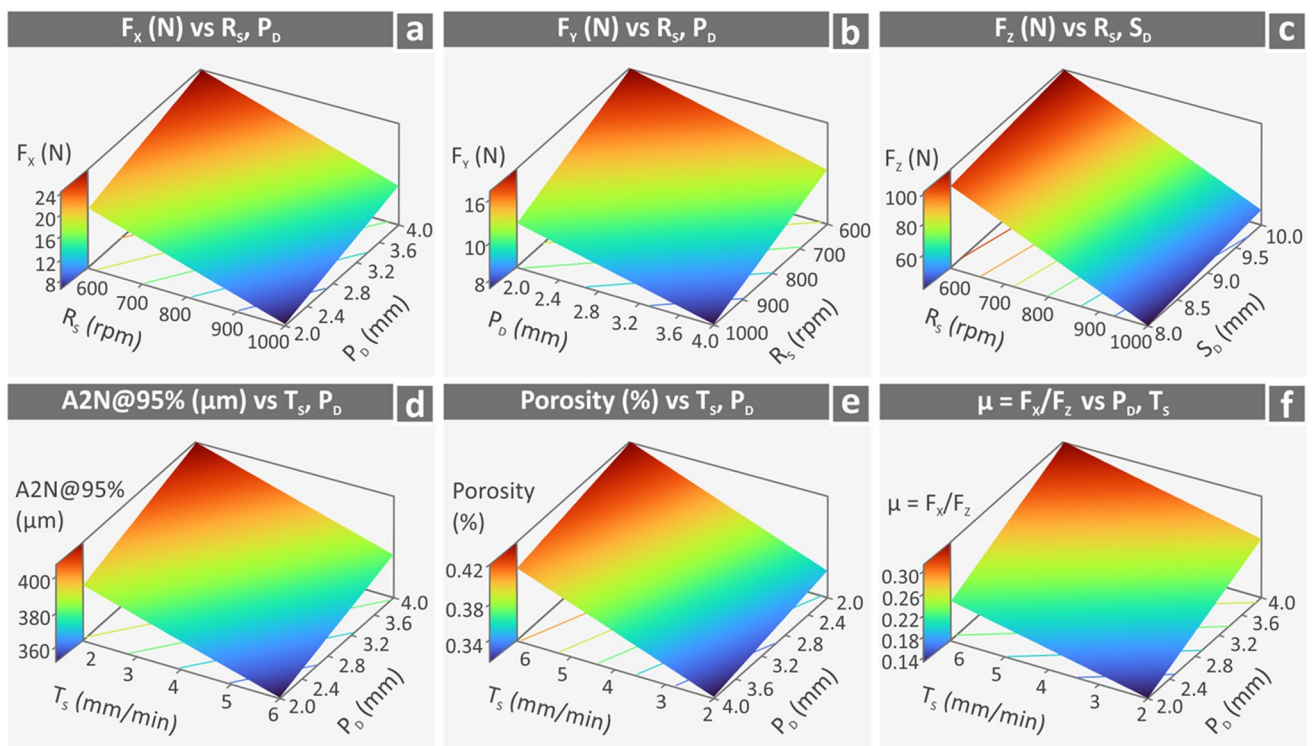


**Fig. 15** Three-dimensional graphs for the response metrics of the study vs. the two most critical control parameters for each response metric **a**  $F_x$ , **b**  $F_y$ , **c**  $F_z$ , **d** A2N@95%, **e** porosity, and **f**  $\mu$

**Table 3** Control parameters and levels for the confirmation run

Run	TS	RS	SD	PD
10	4	1000	10	3

$\mu$ -CT scanning technique was used to assess the porosity of the produced weld and its dimensional accuracy in terms of the control parameters and levels. The aim was to correlate the findings and optimize the process parameters with statistical modeling tools (Taguchi design). Additionally, the results aimed to interpret the mechanical performance of the welded samples and correlate the forces during the process and the produced porosity with the mechanical performance of the weld.  $R_s$  was the most important control parameter affecting the developed force in all directions ( $F_x$ ,  $F_y$ , and  $F_z$ ). The developed forces were similar in the  $F_x$  and the  $F_y$  directions and significantly higher in the  $F_z$  direction. Their values were highly affected by the values of the control parameters with the

highest  $F_x$  force recorded being 350% higher than the lowest one, about the same for the  $F_y$  component and about 215% for the  $F_z$  component. The remaining response metrics of porosity and the dimensional deviation of the created weld seam were not that highly affected by the  $R_s$  control parameter. They were highly affected by the  $T_s$  parameter and the  $P_D$  parameter, showing once again the importance of the weld tool geometry on the produced seam. The difference between the highest and the lowest values reported was about 42% for the porosity and about 25% for the dimensional deviation. Strangely enough, the analysis showed that increased porosity leads to lower dimensional deviation in the produced weld. The highest porosity was reported in Run 9, in which the lowest dimensional deviation was also reported, while the highest dimensional deviation (Run 3) was reported on samples having relatively low porosity. Higher  $T_s$  values lead to increased dimensional accuracy in the seam, while higher  $T_s$  values also develop higher temperatures in the weld

**Table 4** Mean average values and standard deviations of measured responses for force in X axis, force in Y axis, force in Z axis, porosity, and actual to nominal dimensional deviation for the confirmation run

Run	Force X (N)	Force Y (N)	Force Z (N)	Porosity (%)	A2N@95% ( $\mu\text{m}$ )	$\mu$
10	$9.59 \pm 0.78$	$7.52 \pm 0.58$	$62.43 \pm 4.91$	$0.35 \pm 0.02$	$447.48 \pm 23.66$	$0.154 \pm 0.010$

**Table 5** Validation table

Run no.		10
Actual	Force $X$ (N)	9.59
	Force $Y$ (N)	7.52
	Force $Z$ (N)	62.43
	Porosity (%)	0.35
	A2N@95% ( $\mu\text{m}$ )	447.48
	$\mu$	0.15
Predicted	Force $X$ (N)	10.49
	Force $Y$ (N)	7.44
	Force $Z$ (N)	53.36
	Porosity (%)	0.36
	A2N@95% ( $\mu\text{m}$ )	384.22
	$\mu$	0.19
Absolute error	Force $X$ (%)	9.34
	Force $Y$ (%)	1.06
	Force $Z$ (%)	14.53
	Porosity (%)	3.99
	A2N@95% (%)	14.14
	$\mu$ (%)	24.19

(Fig. 12), thus making the material softer, which probably leads to higher dimensional accuracy, considering also the mechanisms reported in the literature in the introduction section [57]. On the other hand, the increased porosity can be probably attributed to the cooling of the polymer from higher temperatures [94–96]. On the other hand, correlating the porosity and the dimensional deviation with the developed forces, no clear connection can be found. Both the highest and the lowest porosity (Runs 9 and 2, respectively) and dimensional accuracy (Runs 3 and 9, respectively) values were achieved in runs, in which the developed forces were rather low. The only obvious connection is that the increased  $T_s$ , which highly affects these two response metrics, increased also the  $F_x$  force.

Regarding the weld tool geometry,  $S_D$  was the least important control parameter affecting the developed forces, while  $P_D$  highly affected the  $F_x$  and the  $F_y$  forces. With the control parameter levels studied, the reported as important in the FSW of aluminum sheets, shoulder-to-pin diameter ratio ranging from 2 to 5. The lowest forces were found with a shoulder-to-pin diameter ratio value of 2.66, while the highest  $F_x$  and  $F_z$  force was found with a shoulder-to-pin diameter ratio value of 3.33 and the higher  $F_y$  with 4. This shows that, although the  $P_D$  affects the developed forces, the extreme shoulder-to-pin diameter ratio values (high or low) do not lead to extreme force values (high or low). Similar outcomes can be assumed for the porosity and the dimensional deviation. The highest porosity was found with a shoulder-to-pin diameter ratio value of 4.5 and the lowest one with 3. The highest dimensional deviation was

found with a shoulder-to-pin diameter ratio value of 2.5 and the lowest one with 4.5. Only the welding resistance rate ( $F_x/F_z$ ) was highly influenced by the shoulder-to-pin diameter ratio, with its lowest value found with the highest shoulder-to-pin diameter ratio value of 5, and its lowest one, with the highest shoulder-to-pin diameter ratio value of 2. This is an indication of the effect of the weld tool geometry on the developed force and the joining mechanisms taking place during the FSW process. This response metric is also highly affected by the  $T_s$  and the  $P_D$  control parameters, with higher values leading to higher welding resistance rate values, following a similar pattern with the temperature (higher temperature values).

By correlating the findings herein for the developed forces, porosity, and dimensional deviation on the FSW of 4 mm PC sheets, with the produced joined samples' mechanical performance from the literature (samples welded with the same FSW conditions) [88], a connection between the response metrics was attempted. The highest tensile strength was achieved in the run (Run 6), which had the lowest developed forces. The highest tensile modulus of elasticity was achieved in the run (Run 7), which had the highest developed  $F_x$  and  $F_z$  forces. The highest flexural strength was achieved in a run (Run 9), which also had rather low developed forces. The highest flexural modulus of elasticity was achieved in a run (Run 8), which similarly to the tensile modulus of elasticity had high  $F_x$  forces, while the  $F_y$  force had a median value, and the  $F_z$  force was rather low. The highest tensile strength was achieved in samples with rather low porosity and median dimensional deviation. The highest tensile modulus of elasticity was achieved in samples with rather high porosity and median dimensional deviation. The highest flexural strength was achieved in samples with high porosity (surprisingly the highest one reported) and the lowest dimensional deviation. The highest flexural modulus of elasticity was achieved in samples with also high porosity and median dimensional deviation. Regarding the welding resistance rate, high values resulted in samples with inferior strength in both the tensile and the flexural test, while low values resulted in average tensile strength and rather high flexural strength values. Regarding the control parameters, the  $R_s$  affecting the developed forces were also the most important parameter affecting the properties of the welded samples in the tensile test. This was also an important parameter for the flexural strength of the samples (ranked as no. 2). This shows a connection between the developed forces and the mechanical strength of the produced weld.  $T_s$  affecting the porosity also leads to reduced tensile and flexural strength at higher values, with parts also having higher porosity percentages. Higher  $P_D$  values increase the dimensional deviation, and the tensile and flexural strength are decreased.

In the literature, to the authors' best knowledge, not much research is available on the developed forces on PC sheets



during the FSW process, and no study investigates the porosity and the dimensional deviation of the produced weld. In a study on 3 mm PC sheets jointed with the FSW process [51], the forces reported are higher than those reported herein. The two studies agree on reporting  $F_x$  and  $F_y$  force components significantly lower than the  $F_z$  ones. Also, the  $F_y$  forces are slightly higher than the  $F_x$  forces in both studies. The difference in the highest force values reported between the two studies can be attributed to several parameters, such as the different PC sheet thickness (3 mm vs. 4 mm), the different grades, and, more importantly, the different FSW parameter values. For example, in [51], the lowest  $R_s$  value (2000 rpm) was two times higher than the  $R_s$  value (1000 rpm) studied herein. It is a common finding in the research of FSW that the FSW parameters highly affect the result of the weld, as mentioned in the literature review section of the current study. Therefore, such differences are expected, but the overall trend is the same in the two studies, verifying the reliability of the process followed and the trustworthiness of the provided results.

## 5 Conclusions

This study focuses on assessing the forces developed during the joining of 4 mm thick PC sheets with the FSW process. The key findings can be summarized as follows:

- $T_s$  highly affects the porosity and the dimensional deviation of the seam (low values reduce porosity to 0.31% and the  $F_x$  force to 8 N, while high values reduce dimensional deviation to 329.97  $\mu\text{m}$  and increase the  $F_x$  force to 28.53 N, which is ~356% higher than the lower force reported).
- In Run 6 ( $T_s$  4 mm/min,  $R_s$  1000 rpm, 2.66 shoulder-to-pin ratio), the lowest forces were developed, i.e.,  $F_x$  8.01 N,  $F_y$  6.32 N, and  $F_z$  48.49 N, while the highest  $F_x$  and  $F_z$  force was developed in Run 7 ( $T_s$  6 mm/min,  $R_s$  600 rpm, 3.33 shoulder-to-pin ratio), i.e.,  $F_x$  28.53 N,  $F_z$  104.82 N.
- The lowest porosity of 0.31% was found in Run 2 ( $T_s$  2 mm/min,  $R_s$  800 rpm, 3 shoulder-to-pin ratio).
- The lowest dimensional deviation of 329.97  $\mu\text{m}$  was found in Run 9 ( $T_s$  6 mm/min,  $R_s$  1000 rpm, 4.5 shoulder-to-pin ratio).
- The lowest welding resistance rate of 0.112 was found in Run 5 ( $T_s$  4 mm/min,  $R_s$  800 rpm, 5 shoulder-to-pin ratio).
- $R_s$  which highly affected the mechanical properties of the welded parts in previous work [88] also affected the developed forces (its increase reduced all, three force metrics and increased the tensile properties), showing a correlation between the developed forces and the mechanical strength of the welded parts.
- In the confirmation run (run no. 10,  $T_s$  4 mm/min,  $R_s$  1000 rpm, 3.33 shoulder-to-pin ratio),  $F_x$  was 9.59 N,  $F_y$

was 7.52 N,  $F_z$  was 62.43 N, porosity was 0.35, dimensional deviation was 447.48  $\mu\text{m}$ , and the welding resistance rate was 0.154. The error from the predicted was good as 1.06% for the  $F_y$  and up to 24.19% for the welding resistance rate, while most values had an error below 10%, showing the reliability of the provided modeling equations and the process followed in total.

The ANOVA prediction models can be directly applied in the industry to predict the expected forces, porosity, and dimensional deviation of PC sheets welded using the FSW process. This information can serve as a guide for selecting appropriate control parameter settings, enabling the production of superior performance and high-quality weld seams. In future research, it is intended to extend the range of control parameter levels and evaluate additional control factors to gain a more comprehensive understanding of the behavior of 4 mm thick PC sheets when joined using the FSW process. Special attention would be given to the control parameters that showed a higher effect on the response metrics.

**Supplementary information** The online version contains supplementary material available at <https://doi.org/10.1007/s00170-024-13033-9>.

**Acknowledgements** The authors would like to thank Aleka Manousaki from the Institute of Electronic Structure and Laser of the Foundation for Research and Technology, Hellas (IESL-FORTH) for taking the SEM images presented in this work.

**Author contribution** NV: conceptualization, methodology, resources, supervision, project administration, writing—review, and editing; MP: methodology, formal analysis, writing—original draft preparation, writing—review, and editing; CD: data curation; DS: data curation and formal analysis; NM: software, formal analysis, investigation, and data curation; AM: investigation and data curation. The manuscript was written through the contributions of all authors. All authors have approved the final version of the manuscript.

**Funding** Open access funding provided by HEAL-Link Greece.

**Data availability** The raw/processed data required to reproduce these findings cannot be shared at this time due to technical or time limitations.

## Declarations

**Conflict of interest** The authors declare no competing interests.

**Open Access** This article is licensed under a Creative Commons Attribution 4.0 International License, which permits use, sharing, adaptation, distribution and reproduction in any medium or format, as long as you give appropriate credit to the original author(s) and the source, provide a link to the Creative Commons licence, and indicate if changes were made. The images or other third party material in this article are included in the article's Creative Commons licence, unless indicated otherwise in a credit line to the material. If material is not included in the article's Creative Commons licence and your intended use is not permitted by statutory regulation or exceeds the permitted use, you will need to obtain permission directly from the copyright holder. To view a copy of this licence, visit <http://creativecommons.org/licenses/by/4.0/>.

## References

- Threadgill PL, Leonard AJ, Shercliff HR, Withers PJ (2009) Friction stir welding of aluminium alloys. *Int Mater Rev* 54:49–93. <https://doi.org/10.1179/174328009X411136>
- Chien CH, Lin WB, Chen T (2011) Optimal FSW process parameters for aluminum alloys AA5083. *J Chin Ins Eng Trans Chin Ins Eng Ser A* 34:99–105. <https://doi.org/10.1080/02533839.2011.553024>
- Vidakis N, Vairis A, Diouf D et al (2016) Effect of the tool rotational speed on the mechanical properties of thin AA1050 friction stir welded sheets. *J Eng Sci Technol Rev* 9(3):123–129
- Heinz B, Skrotzki B (2002) Characterization of a friction-stir-welded aluminum alloy 6013. *Metall Mater Trans B: Process Metall Mater Process Sci* 33:489–498. <https://doi.org/10.1007/s11663-002-0059-5>
- Sakthivel T, Sengar GS, Mukhopadhyay J (2009) Effect of welding speed on microstructure and mechanical properties of friction-stir-welded aluminum. *Int J Adv Manuf Tech* 43:468–473. <https://doi.org/10.1007/s00170-008-1727-7>
- Fujii H, Cui L, Maeda M, Nogi K (2006) Effect of tool shape on mechanical properties and microstructure of friction stir welded aluminum alloys. *Mater Sci Eng A* 419:25–31. <https://doi.org/10.1016/j.msea.2005.11.045>
- Dimopoulos A, Vairis A, Vidakis N, Petousis M (2021) On the friction stir welding of al 7075 thin sheets. *Metals (Basel)* 11:1–12. <https://doi.org/10.3390/met11010057>
- Mironov S, Inagaki K, Sato YS, Kokawa H (2015) Effect of welding temperature on microstructure of friction-stir welded aluminum alloy 1050. *Metall Mater Trans A Phys Metall Mater Sci* 46:783–790. <https://doi.org/10.1007/s11661-014-2651-0>
- Li H, Gao J, Li Q (2018) Fatigue of friction stir welded aluminum alloy joints: a review. *Appl Sci* 8(12):2626. <https://doi.org/10.3390/app8122626>
- Suresh S, Natarajan E, Franz G, Rajesh S (2022) Differentiation in the SiC filler size effect in the mechanical and tribological properties of friction-spot-welded AA5083-H116 alloy. *Fibers* 10(12):109. <https://doi.org/10.3390/fib10120109>
- Abdollahzadeh A, Bagheri B, Abbasi M et al (2021) A modified version of friction stir welding process of aluminum alloys: analyzing the thermal treatment and wear behavior. *Proc Inst Mech Eng Part L: J Mater Des Appl* 235:2291–2309. <https://doi.org/10.1177/14644207211023987>
- Abbasi M, Givi M, Bagheri B (2020) New method to enhance the mechanical characteristics of Al-5052 alloy weldment produced by tungsten inert gas. *Proc Inst Mech Eng B J Eng Manuf*. <https://doi.org/10.1177/0954405420929777>
- Bagheri B, Abdollahzadeh A, Sharifi F et al (2021) RETRACTED: recent development in friction stir processing of aluminum alloys: microstructure evolution, mechanical properties, wear and corrosion behaviors. *Proc Ins Mech Eng Part E: J Process Mech Eng*. <https://doi.org/10.1177/09544089211058007>
- Bagheri B, Sharifi F, Abbasi M, Abdollahzadeh A (2021) On the role of input welding parameters on the microstructure and mechanical properties of Al6061-T6 alloy during the friction stir welding: experimental and numerical investigation. *Proc Inst Mech Eng Part L: J Mater Des Appl* 236:299–318. <https://doi.org/10.1177/14644207211044407>
- Abbasi M, Bagheri B, Abdollahzadeh A, Moghaddam AO (2021) A different attempt to improve the formability of aluminum tailor welded blanks (TWB) produced by the FSW. *Int J Mater Form* 14:1189–1208. <https://doi.org/10.1007/s12289-021-01632-w>
- Abbasi M, Abdollahzadeh A, Bagheri B et al (2021) Study on the effect of the welding environment on the dynamic recrystallization phenomenon and residual stresses during the friction stir welding process of aluminum alloy. *Proc Inst Mech Eng Part L: J Mater Des Appl* 235:1809–1826. <https://doi.org/10.1177/14644207211025113>
- Abdollahzadeh A, Bagheri B, Abbasi M et al (2021) Comparison of the weldability of AA6061-T6 joint under different friction stir welding conditions. *J Mater Eng Perform* 30:1110–1127. <https://doi.org/10.1007/s11665-020-05379-4>
- Bagheri B, Abbasi M, Abdollahzadeh A (2021) Microstructure and mechanical characteristics of AA6061-T6 joints produced by friction stir welding, friction stir vibration welding and tungsten inert gas welding: a comparative study. *Int J Min Metall Mater* 28:450–461. <https://doi.org/10.1007/s12613-020-2085-1>
- Bagheri B, Abbasi M, Hamzeloo R (2020) Comparison of different welding methods on mechanical properties and formability behaviors of tailor welded blanks (TWB) made from AA6061 alloys. *Proc Inst Mech Eng C J Mech Eng Sci* 235:2225–2237. <https://doi.org/10.1177/0954406220952504>
- Suresh S, Elango N, Venkatesan K et al (2020) Sustainable friction stir spot welding of 6061–T6 aluminium alloy using improved non-dominated sorting teaching learning algorithm. *J Mater Res Technol* 9:11650–11674. <https://doi.org/10.1016/j.jmrt.2020.08.043>
- Suresh S, Venkatesan K, Rajesh S (2019) Optimization of process parameters for friction stir spot welding of AA6061/Al2O3 by Taguchi method. *AIP Conf Proc* 2128:30018. <https://doi.org/10.1063/1.5117961>
- Suresh S, Natarajan E, Vinayagamurthi P et al (2023) Optimum tool traverse speed resulting equiaxed recrystallized grains and high mechanical strength at swept friction stir spot welded AA7075-T6 lap joints BT - Materials, Design and Manufacturing for Sustainable Environment. In: Vinodh S, Rajkumar V (eds) Natarajan E. Springer Nature Singapore, Singapore, pp 547–555
- Suresh S, Venkatesan K, Natarajan E, Rajesh S (2021) Performance analysis of nano silicon carbide reinforced swept friction stir spot weld joint in AA6061-T6 alloy. *Silicon* 13:3399–3412. <https://doi.org/10.1007/s12633-020-00751-4>
- Bagheri B, Abbasi M, Dadaei M (2020) Mechanical behavior and microstructure of AA6061-T6 joints made by friction stir vibration welding. *J Mater Eng Perform* 29:1165–1175. <https://doi.org/10.1007/s11665-020-04639-7>
- Abbasi M, Bagheri B, Sharifi F (2021) Simulation and experimental study of dynamic recrystallization process during friction stir vibration welding of magnesium alloys. *Trans Nonferrous Metals Soc Chin* 31:2626–2650. [https://doi.org/10.1016/S1003-6326\(21\)65681-9](https://doi.org/10.1016/S1003-6326(21)65681-9)
- Antoniadis A, Vidakis N, Bilalis N (2002) Fatigue fracture investigation of cemented carbide tools in gear hobbing, Part 2: the effect of cutting parameters on the level of tool stresses - a quantitative parametric analysis. *J Manuf Sci Eng* 124:792–798. <https://doi.org/10.1115/1.1511173>
- Bagheri B, Abbasi M, Abdollahzadeh A, Kokabi AH (2020) Numerical analysis of cooling and joining speed effects on friction stir welding by smoothed particle hydrodynamics (SPH). *Arch App Mech* 90:2275–2296. <https://doi.org/10.1007/s00419-020-01720-4>
- Vairis A, Petousis M, Mountakis N et al (2022) The effect of tool geometry on the strength of FSW aluminum thin sheets. *Materials* 15:8187. <https://doi.org/10.3390/ma15228187>
- Trimble D, Monaghan J, O'Donnell GE (2012) Force generation during friction stir welding of AA2024-T3. *CIRP Annals* 61:9–12. <https://doi.org/10.1016/j.cirp.2012.03.024>
- Lambiase F, Paoletti A, Di Ilio A (2018) Forces and temperature variation during friction stir welding of aluminum alloy AA6082-T6. *Int J Adv Manuf Technol* 99:337–346. <https://doi.org/10.1007/s00170-018-2524-6>
- Liu Z, Guan W, Li H et al (2022) Study on the relationship between welding force and defects in bobbin tool friction stir

- welding. *J Manuf Process* 84:1122–1132. <https://doi.org/10.1016/j.jmapro.2022.10.069>
32. Assidi M, Fourment L, Guerdoux S, Nelson T (2010) Friction model for friction stir welding process simulation: calibrations from welding experiments. *Int J Mach Tools Manuf* 50:143–155. <https://doi.org/10.1016/j.ijmactools.2009.11.008>
  33. Vidakis N, Petousis M, Mountakis N, Karapidakis E (2023) Box-Behnken modeling to quantify the impact of control parameters on the energy and tensile efficiency of PEEK in MEX 3D-printing. *Heliyon* 9(7):e18363. <https://doi.org/10.1016/j.heliyon.2023.e18363>
  34. Kumar S, Mahajan A, Kumar S, Singh H (2022) Friction stir welding: types, merits & demerits, applications, process variables & effect of tool pin profile. *Mater Today Proc* 56:3051–3057. <https://doi.org/10.1016/j.matpr.2021.12.097>
  35. Eslami S, Tavares PJ, Moreira PMGP (2017) Friction stir welding tooling for polymers: review and prospects. *Int J Adv Manuf Technol* 89:1677–1690. <https://doi.org/10.1007/s00170-016-9205-0>
  36. Mishra D, Sahu SK, Mahto RP, Pal SK, Pal K (2020) Friction stir welding for joining of polymers. *Lecture Notes on Multidisciplinary Industrial Engineering*. Springer, Singapore. [https://doi.org/10.1007/978-981-13-0378-4\\_6](https://doi.org/10.1007/978-981-13-0378-4_6)
  37. Huang Y, Meng X, Xie Y et al (2018) Friction stir welding/processing of polymers and polymer matrix composites. *Compos Part A Appl Sci Manuf* 105:235–257. <https://doi.org/10.1016/j.compositesa.2017.12.005>
  38. Kumar R, Singh R, Ahuja IPS et al (2018) Weldability of thermoplastic materials for friction stir welding- a state of art review and future applications. *Compos B Eng* 137:1–15. <https://doi.org/10.1016/j.compositesb.2017.10.039>
  39. Nath RK, Maji P, Barma JD (2022) Effect of tool rotational speed on friction stir welding of polymer using self-heated tool. *Production Engineering* 16:683–690. <https://doi.org/10.1007/s11740-022-01123-0>
  40. Khalaf HI, Al-Sabur R, Demiral M et al (2022) The effects of pin profile on HDPE thermomechanical phenomena during FSW. *Polymers (Basel)* 14(21):4632. <https://doi.org/10.3390/polym14214632>
  41. Elyasi M, Derazkola HA (2018) Experimental and thermo-mechanical study on FSW of PMMA polymer T-joint. *Int J Adv Manuf Technol* 97:1445–1456. <https://doi.org/10.1007/s00170-018-1847-7>
  42. Arif M, Kumar D, Siddiquee AN (2023) Mechanical properties and defects in friction stir welded acrylonitrile butadiene styrene polymer. *Proc Inst Mech Eng Part L: J Mater Des Appl* 237(9):1897–1909. <https://doi.org/10.1177/14644207231161189>
  43. Kumari S, Bandhu D, Muchhadiya A, Abhishek K (2023) Recent trends in parametric influence and microstructural analysis of friction stir welding for polymer composites. *Adv Mater Process Technol* 00:1–21. <https://doi.org/10.1080/2374068X.2023.2193447>
  44. Kumar S, Roy BS (2022) A comparative analysis on friction stir welding of similar and dissimilar polymers: acrylonitrile butadiene styrene and polycarbonate plates. *Weld World* 66:1141–1153. <https://doi.org/10.1007/s40194-022-01294-5>
  45. Barakat AA, Darras BM, Nazzal MA, Ahmed AA (2023) A comprehensive technical review of the friction stir welding of metal-to-polymer hybrid structures. *Polymers (Basel)* 15(1):220. <https://doi.org/10.3390/polym15010220>
  46. Correia AN, Santos PAM, Braga DFO et al (2023) Effects of processing temperature on failure mechanisms of dissimilar aluminum-to-polymer joints produced by friction stir welding. *Eng Fail Anal* 146:107155. <https://doi.org/10.1016/j.engfailanal.2023.107155>
  47. Singh S, Prakash C, Gupta MK (2020) On friction-stir welding of 3D printed thermoplastics. In: Gupta K (ed) *Materials forming, machining and post processing*. Materials forming, machining and tribology. Springer, Cham, pp 75–91. [https://doi.org/10.1007/978-3-030-18854-2\\_3](https://doi.org/10.1007/978-3-030-18854-2_3)
  48. Iftikhar SH, Mourad AHI, Sheikh-Ahmad J et al (2021) A comprehensive review on optimal welding conditions for friction stir welding of thermoplastic polymers and their composites. *Polymers (Basel)* 13(8):1208. <https://doi.org/10.3390/polym13081208>
  49. Petousis M, Mountakis N, Vidakis N (2023) Optimization of hybrid friction stir welding of PMMA: 3D-printed parts and conventional sheets welding efficiency in single- and two-axis welding traces. *Int J Adv Manuf Technol*. <https://doi.org/10.1007/s00170-023-11632-6>
  50. Vidakis N, Petousis M, Mountakis N, Kechagias JD (2022) Material extrusion 3D printing and friction stir welding: an insight into the weldability of polylactic acid plates based on a full factorial design. *Int J Adv Manuf Technol* 121:3817–3839. <https://doi.org/10.1007/s00170-022-09595-1>
  51. Lambiase F, Paoletti A, Grossi V, Di Ilio A (2019) Analysis of loads, temperatures and welds morphology in FSW of polycarbonate. *J Mater Process Technol* 266:639–650. <https://doi.org/10.1016/j.jmatprotec.2018.11.043>
  52. Vidakis N, Petousis M, Korlos A et al (2022) Friction stir welding optimization of 3D-printed acrylonitrile butadiene styrene in hybrid additive manufacturing. *Polymers (Basel)* 14:2474. <https://doi.org/10.3390/polym14122474>
  53. Vidakis N, Petousis M, Mountakis N, Kechagias JD (2022) Optimization of friction stir welding for various tool pin geometries: the weldability of Polyamide 6 plates made of material extrusion additive manufacturing. *Int J Adv Manuf Technol*. <https://doi.org/10.1007/s00170-022-10675-5>
  54. Vidakis N, Petousis M, Mountakis N, Kechagias JD (2022) Optimization of friction stir welding parameters in hybrid additive manufacturing: weldability of 3D-printed poly(methyl methacrylate) plates. *J Manuf Mater Process* 6(4):77. <https://doi.org/10.3390/jmmp6040077>
  55. Sheikh-Ahmad JY, Ali DS, Devenci S et al (2019) Friction stir welding of high density polyethylene—carbon black composite. *J Mater Process Technol* 264:402–413. <https://doi.org/10.1016/j.jmatprotec.2018.09.033>
  56. Paoletti A, Lambiase F, Di Ilio A (2016) Analysis of forces and temperatures in friction spot stir welding of thermoplastic polymers. *Int J Adv Manuf Technol* 83:1395–1407. <https://doi.org/10.1007/s00170-015-7669-y>
  57. Guan W, Zhao Y, Liu Y et al (2022) Force data-driven machine learning for defects in friction stir welding. *Scr Mater* 217:114765. <https://doi.org/10.1016/j.scriptamat.2022.114765>
  58. Stadler GR, Szabéni G, Horváth R (2023) Investigation of weld forces and strength of friction stir welded polypropylene. *Period Polytech Mech Eng* 67:183–189. <https://doi.org/10.3311/PPme.21899>
  59. Eslami S, Ramos T, Tavares PJ, Moreira PMGP (2015) Effect of friction stir welding parameters with newly developed tool for lap joint of dissimilar polymers. *Procedia Eng* 114:199–207. <https://doi.org/10.1016/j.proeng.2015.08.059>
  60. Eslami S, Mourão L, Viriato N et al (2018) Multi-axis force measurements of polymer friction stir welding. *J Mater Process Technol* 256:51–56. <https://doi.org/10.1016/j.jmatprotec.2018.01.044>
  61. Dialami N, Chiumentini M, Cervera M et al (2017) Enhanced friction model for friction stir welding (FSW) analysis: Simulation and experimental validation. *Int J Mech Sci* 133:555–567. <https://doi.org/10.1016/j.ijmeosci.2017.09.022>
  62. Schmauder T, Nauenburg KD, Kruse K, Ickes G (2006) Hard coatings by plasma CVD on polycarbonate for automotive and optical applications. *Thin Solid Films* 502:270–274. <https://doi.org/10.1016/j.tsf.2005.07.296>
  63. Pan K, Zhang W, Shi H et al (2022) Zinc Ion-crosslinked polycarbonate/heparin composite coatings for biodegradable Zn-alloy

- stent applications. *Colloids Surf B Biointerfaces* 218:112725. <https://doi.org/10.1016/j.colsurfb.2022.112725>
64. Pedrosa P, Alves E, Barradas NP et al (2012) TiN x coated polycarbonate for bio-electrode applications. *Corros Sci* 56:49–57. <https://doi.org/10.1016/j.corsci.2011.11.008>
  65. Jadhav VD, Patil AJ, Kandasubramanian B (2022) Polycarbonate nanocomposites for high impact applications BT - handbook of consumer nanoproducts. In: Hussain CM (ed) Mallakpour S. Springer Nature Singapore, Singapore, pp 257–281
  66. Kausar A (2018) A review of filled and pristine polycarbonate blends and their applications. *J Plast Film Sheeting* 34:60–97. <https://doi.org/10.1177/8756087917691088>
  67. Vidakis N, Petousis M, Kechagias JD (2022) A comprehensive investigation of the 3D printing parameters' effects on the mechanical response of polycarbonate in fused filament fabrication. *Prog Addit Manuf* 7:713–722. <https://doi.org/10.1007/s40964-021-00258-3>
  68. Vidakis N, Petousis M, Korlos A et al (2021) Strain rate sensitivity of polycarbonate and thermoplastic polyurethane for various 3D printing temperatures and layer heights. *Polymers (Basel)* 13:2752. <https://doi.org/10.3390/polym13162752>
  69. Vidakis N, Petousis M, Velidakis E et al (2021) Mechanical performance of fused filament fabricated and 3d-printed polycarbonate polymer and polycarbonate/ cellulose nanofiber nanocomposites. *Fibers* 9:74. <https://doi.org/10.3390/fib9110074>
  70. Vidakis N, Petousis M, Mangelis P et al (2022) Thermomechanical response of polycarbonate/aluminum nitride nanocomposites in material extrusion additive manufacturing. *Materials* 15(24):8806. <https://doi.org/10.3390/ma15248806>
  71. Petousis M, Vidakis N, Mountakis N et al (2022) Silicon carbide nanoparticles as a mechanical boosting agent in material extrusion 3D-printed polycarbonate. *Polymers (Basel)* 14:1–20. <https://doi.org/10.3390/polym14173492>
  72. Vidakis N, Petousis M, Mountakis N et al (2022) On the thermal and mechanical performance of polycarbonate / titanium nitride nanocomposites in material extrusion additive manufacturing. *Compos Part C: Open Access* 8:100291. <https://doi.org/10.1016/j.jcomc.2022.100291>
  73. Vidakis N, Petousis M, Grammatikos S et al (2022) High performance polycarbonate nanocomposites mechanically boosted with titanium carbide in material extrusion additive manufacturing. *Nanomaterials* 12:1068. <https://doi.org/10.3390/nano12071068>
  74. Vidakis N, Petousis M, David CN et al (2023) Mechanical performance over energy expenditure in MEX 3D printing of polycarbonate: a multiparametric optimization with the aid of robust experimental design. *J Manuf Mater Process* 7:38. <https://doi.org/10.3390/jmmp7010038>
  75. Vidakis N, Petousis M, Mountakis N et al (2023) Mechanical strength predictability of full factorial, Taguchi, and box Behnken designs: optimization of thermal settings and cellulose nanofibers content in PA12 for MEX AM. *J Mech Behav Biomed Mater* 142:105846. <https://doi.org/10.1016/j.jmbbm.2023.105846>
  76. Petousis M, Vidakis N, Mountakis N et al (2023) Functionality versus sustainability for PLA in MEX 3D printing : the impact of generic process control factors on flexural response and energy efficiency. *Polymers (Basel)* 15:1232. <https://doi.org/10.3390/polym15051232>
  77. David C, Sagris D, Petousis M et al (2023) Operational performance and energy efficiency of MEX 3D printing with polyamide 6 (PA6): multi-objective optimization of seven control settings supported by L27 robust design. *App Sci* 13(15):8819. <https://doi.org/10.3390/app13158819>
  78. Vidakis N, David CN, Petousis M et al (2022) Optimization of key quality indicators in material extrusion 3D printing of acrylonitrile butadiene styrene: the impact of critical process control parameters on the surface roughness, dimensional accuracy, and porosity. *Mater Today Commun* 34:105171. <https://doi.org/10.1016/j.mtcomm.2022.105171>
  79. Petousis M, Vidakis N, Mountakis N et al (2023) Compressive response versus power consumption of acrylonitrile butadiene styrene in material extrusion additive manufacturing : the impact of seven critical control parameters. *J Adv Manuf Technol*. <https://doi.org/10.1007/s00170-023-11202-w>
  80. Derazkola HA, Khodabakhshi F (2020) Development of fed friction-stir (FFS) process for dissimilar nanocomposite welding between AA2024 aluminum alloy and polycarbonate (PC). *J Manuf Process* 54:262–273. <https://doi.org/10.1016/j.jmapro.2020.03.020>
  81. Ahmed MMZ, Elnaml A, Shazly M, El-Sayed Seleman MM (2021) The effect of top surface lubrication on the friction stir welding of polycarbonate sheets. *Int Polym Process* 36:94–102. <https://doi.org/10.1515/ipp-2020-3991>
  82. Lambiase F, Grossi V, Paoletti A (2020) Effect of tilt angle in FSW of polycarbonate sheets in butt configuration. *Int J Adv Manuf Technol* 107:489–501. <https://doi.org/10.1007/s00170-020-05106-2>
  83. Lambiase F, Grossi V, Paoletti A (2019) Advanced mechanical characterization of friction stir welds made on polycarbonate. *Int J Adv Manuf Technol* 104:2089–2102. <https://doi.org/10.1007/s00170-019-04006-4>
  84. Lambiase F, Paoletti A, Di Ilio A (2016) Effect of tool geometry on loads developing in friction stir spot welds of polycarbonate sheets. *Int J Adv Manuf Technol* 87:2293–2303. <https://doi.org/10.1007/s00170-016-8629-x>
  85. Meena SL, Murtaza Q, Walia RS et al (2021) Modelling and simulation of FSW of polycarbonate using finite element analysis. *Mater Today Proc* 50:2424–2429. <https://doi.org/10.1016/j.matpr.2021.10.260>
  86. Derazkola HA, Eyvazian A, Simchi A (2020) Modeling and experimental validation of material flow during FSW of polycarbonate. *Mater Today Commun* 22:100796. <https://doi.org/10.1016/j.mtcomm.2019.100796>
  87. Shazly M, Ahmed MMZ, El-Raey M (2014) Friction stir welding of polycarbonate sheets. In: Carpenter JS, Bai C, Hwang J-Y, Ikhmayies S, Li B, Monteiro SN, Peng Z, Zhang M (eds) TMS annual meeting, pp 555–564. <https://doi.org/10.1002/9781118888056.ch65>
  88. Vidakis N, Mountakis N, Moutsopoulou A et al (2023) The impact of process parameters and pin-to-shoulder diameter ratio on the welding performance of polycarbonate in FSW. *Int J Adv Manuf Technol*. <https://doi.org/10.1007/s00170-023-12192-5>
  89. Eslami S, Ramos T, Tavares PJ, Moreira PMGP (2015) Shoulder design developments for FSW lap joints of dissimilar polymers. *J Manuf Process* 20:15–23. <https://doi.org/10.1016/j.jmapro.2015.09.013>
  90. Khan NZ, Khan ZA, Siddiquee AN (2015) Effect of Shoulder diameter to pin diameter (D/d) ratio on tensile strength of friction stir welded 6063 aluminium alloy. *Mater Today Proc* 2:1450–1457. <https://doi.org/10.1016/j.matpr.2015.07.068>
  91. Phadke MS (1995) Quality engineering using robust design, 1st edn. Prentice Hall PTR, USA
  92. Swamidass PM (ed) (2000) Mean absolute percentage error (MAPE). In: Encyclopedia of production and manufacturing management. Springer US, Boston, p 462. [https://doi.org/10.1007/1-4020-0612-8\\_580](https://doi.org/10.1007/1-4020-0612-8_580)
  93. White KJ (1992) The Durbin-Watson test for autocorrelation in nonlinear models. *Rev Econ Stat* 74:370–373. <https://doi.org/10.2307/2109675>
  94. Marascio MGM, Antons J, Pioletti DP, Bourban P-E (2017) 3D printing of polymers with hierarchical continuous porosity. *Adv Mater Technol* 2:1700145. <https://doi.org/10.1002/admt.201700145>
  95. Hentze H-P, Antonietti M (2002) Porous polymers and resins for biotechnological and biomedical applications. *Rev Molec*

Biotechnol 90:27–53. [https://doi.org/10.1016/S1389-0352\(01\)00046-0](https://doi.org/10.1016/S1389-0352(01)00046-0)

96. Nam YS, Park TG (1999) Porous biodegradable polymeric scaffolds prepared by thermally induced phase separation. J Biomed Mater Res 47:8–17. [https://doi.org/10.1002/\(SICI\)1097-4636\(199910\)47:1%3c8::AID-JBM2%3e3.0.CO;2-L](https://doi.org/10.1002/(SICI)1097-4636(199910)47:1%3c8::AID-JBM2%3e3.0.CO;2-L)

**Publisher's Note** Springer Nature remains neutral with regard to jurisdictional claims in published maps and institutional affiliations.